



UNIVERSITY OF LEEDS

This is a repository copy of *A short motif in the N-terminal region of α -synuclein is critical for both aggregation and function.*

White Rose Research Online URL for this paper:

<https://eprints.whiterose.ac.uk/155980/>

Version: Accepted Version

Article:

Doherty, CPA orcid.org/0000-0001-5685-4716, Ulamec, SM orcid.org/0000-0002-9415-753X, Maya-Martinez, R orcid.org/0000-0002-7371-8051 et al. (6 more authors) (2020) A short motif in the N-terminal region of α -synuclein is critical for both aggregation and function. *Nature Structural & Molecular Biology*, 27. pp. 249-259. ISSN 1545-9993

<https://doi.org/10.1038/s41594-020-0384-x>

Reuse

Items deposited in White Rose Research Online are protected by copyright, with all rights reserved unless indicated otherwise. They may be downloaded and/or printed for private study, or other acts as permitted by national copyright laws. The publisher or other rights holders may allow further reproduction and re-use of the full text version. This is indicated by the licence information on the White Rose Research Online record for the item.

Takedown

If you consider content in White Rose Research Online to be in breach of UK law, please notify us by emailing eprints@whiterose.ac.uk including the URL of the record and the reason for the withdrawal request.



eprints@whiterose.ac.uk
<https://eprints.whiterose.ac.uk/>

1 ***A short motif in the N-terminal region of α -synuclein is critical for both***
2 ***aggregation and function***

3

4 **Ciaran P. A. Doherty^{1,2}, Sabine M. Ulamec^{1,2}, Roberto Maya-Martinez¹, Sarah C. Good¹,**
5 **Jemma Makepeace¹, G. Nasir Khan¹, Patricija van Oosten-Hawle¹, Sheena E. Radford^{1,*},**
6 **David J. Brockwell^{1,*}**

7

8 ¹ Astbury Centre for Structural Molecular Biology, School of Molecular and Cellular Biology, Faculty
9 of Biological Sciences, University of Leeds, LS2 9JT, United Kingdom

10 ² joint first authors

11 * Corresponding authors:

12 Sheena E Radford

13 Tel: +113 343 3170, Email: S.E.Radford@leeds.ac.uk

14

15 David J Brockwell

16 Tel: +113 343 7821; Email: D.J.Brockwell@leeds.ac.uk

17

18

19 **Abstract**

20 Aggregation of human α -synuclein (α Syn) is linked to Parkinson's disease (PD) pathology. The central
21 region of the α Syn sequence contains the non-amyloid β -component (NAC) crucial for aggregation.
22 However, how NAC flanking regions modulate α Syn aggregation remains unclear. Using
23 bioinformatics, mutation, and NMR we identify a 7-residue sequence, named P1 (residues 36-42),
24 that controls α Syn aggregation. Deletion or substitution of this 'master-controller' prevents
25 aggregation at pH 7.5 *in vitro*. At lower pH, P1 synergises with a sequence containing the PreNAC
26 region (P2, residues 45-57) to prevent aggregation. Deleting P1 (Δ P1) or both P1 and P2 ($\Delta\Delta$) also
27 prevents age-dependent α Syn aggregation and toxicity in *C. elegans* models and prevents α Syn-
28 mediated vesicle fusion by altering the conformational properties of the protein when lipid-bound.
29 The results highlight the importance of a master-controller sequence motif that controls both α Syn
30 aggregation and function- a region that could be targeted to prevent aggregation in disease.

31

32 Introduction

33 The aggregation of α -synuclein (α Syn), a neuronal protein with a primary locus at pre-synaptic nerve
34 termini of the central nervous system¹, is closely associated with Parkinson's disease (PD) and other
35 synucleinopathies^{2,3}. PD affects more than 1% of the world population over the age of 60 and 10
36 million people worldwide⁴. The aetiology of PD and the processes by which α Syn self-assembles to
37 and causes toxicity is not fully understood. For example, while monomeric α Syn is intrinsically
38 disordered *in vitro* and *in vivo*^{5,6}, it forms an array of oligomers^{7,8} and fibril structures⁹, only some of
39 which are cytotoxic or infectious⁷.

40 The primary sequence of α Syn comprises three regions (Figure 1A). The N-terminal region (residues
41 1-60), is basic and contains 6 to 9 conserved imperfect repeats (KTKEGV) crucial for membrane
42 binding¹⁰. The central NAC region (residues 61-95), has been shown to be necessary and sufficient
43 for the aggregation of α Syn^{11,12}. This region also forms the core of some, but not all, α Syn amyloid
44 fibril structures¹³⁻¹⁵. Finally, the C-terminal region (residues 96-140) is highly flexible and enriched in
45 acidic residues. Although α Syn is an intrinsically disordered protein (IDP), it has a smaller radius of
46 gyration¹⁶⁻¹⁸ and collisional cross section¹⁹ than expected for a 140-residue random coil²⁰. Its
47 compaction is driven by transient long range electrostatic and hydrophobic interactions between the
48 chemically distinct domains^{17,21}. Given its distinct charge patterning (12 basic residues in the N-
49 terminal region and 15 acidic residues in the C-terminal region), the conformational properties of
50 α Syn are dependent on the solution pH and ionic strength^{16-18,21}, which in turn affect the aggregation
51 rate of the NAC region^{22,23}.

52 The effects of sequence changes on the conformational properties and aggregation rates of IDPs
53 have been widely studied²⁴⁻²⁸. Notably for α Syn, the seven known familial point mutations that lead
54 to early onset PD are clustered in a region (residues 30-53) that flanks NAC (Figure 1A). Deletion of
55 two of the imperfect repeats (residues 9-30), or truncation of the C-terminal region by 11 to 37
56 residues, increase the rate of α Syn aggregation²⁹⁻³¹, while insertion of two additional N-terminal
57 imperfect repeats (by duplication of residues 9-30) inhibits aggregation³⁰, highlighting the important,
58 but complex, roles of these regions in modulating assembly. Other studies have suggested that the
59 region preceding NAC (residues 47-56, known as PreNAC) is an important modulator of α Syn
60 aggregation, as this region contains the familial mutations and is able to aggregate into amyloid-like
61 fibrils in isolation³². This sequence also forms the inter-protofilament interface in some^{13,14,33}, but not
62 all¹³, α Syn amyloid fibril structures. However, the molecular mechanism(s) by which this region
63 modulates assembly remain unclear.

64 Here, we used *in silico* methods to identify two sequence motifs named P1 (residues 36-42) and P2
65 (residues 45-57) in the N-terminal region of α Syn that have limited solubility and significant
66 aggregation propensity. We show that these regions are critical for aggregation *in vitro* and when
67 expressed *in vivo* as a α Syn-YFP fusion in the bodywall muscle cells of *C. elegans*³⁴. Paramagnetic
68 relaxation enhancement (PRE) NMR experiments reveal pH- and salt-dependent interactions of
69 these motifs with the NAC and C-terminal regions of the protein, the presence of which correlates
70 with an increased aggregation rate. Finally, we show that P1 and P2 are important for α Syn-
71 mediated membrane fusion^{35,36}, since their deletion prevents lipid tubule formation and alters the
72 structure of the lipid-bound protein. Together, the results identify P1 as the 'master-controller' of
73 α Syn aggregation as this region governs the conformational properties and aggregation propensity
74 of α Syn at neutral pH. This region also acts synergistically with P2 (PreNAC) to control assembly at
75 low (lysosomal) pH. The results portray the tug-of-war between function and aggregation in this IDP,
76 with the presence of the P1/P2 regions being essential for vesicle fusion, while simultaneously
77 enhancing amyloid formation.

78

79 Results

80 Identification of the P1 and P2 motifs in the N-terminal region of α Syn

81 To investigate the role of the flanking regions of α Syn in aggregation we analysed its sequence
82 (Figure 1a) using Zyggregator (amyloid propensity³⁷); Camsol (local solubility³⁸) and ZipperDB (β -
83 zipper propensity³⁹) (Figure 1b-e). This revealed three sequences in the N-terminal region predicted
84 to have low solubility (similar to NAC): ²DVFMKGL⁷, ³⁶GVLVGS⁴² (named P1) and
85 ⁴⁵KEGVVHGVATVAE⁵⁷ (named P2). These regions also have high amyloid propensity as judged by
86 Zyggregator, while ZipperDB identified P2, but not P1 or the N-terminal segment as aggregation-
87 prone. Since the role of the N-terminal region of α Syn (residues 1-30) has previously been studied by
88 characterisation of deletion⁴⁰ and extension³⁰ variants, this region was not considered further here.
89 The PreNAC region (residues 47-56) was identified by Eisenberg and colleagues³² and forms part of
90 P2 (residues 45-57). This region also contains six of the seven known familial PD point mutations
91 (Figure 1a). Previous studies have identified a potential role for the P1 and P2 regions in α Syn
92 aggregation, with 47-56 forming amyloid-like aggregates in isolation³², while others have shown that
93 inducing β -hairpin formation in the P1/P2 region (residues ³⁷VLYVGSK⁴³ and ⁴⁸VVHGVAT⁵⁴) stabilised
94 by binding to a β -wrapin (an engineered binding protein) prevents fibril formation⁴¹⁻⁴³. Precisely
95 how these sequences affect aggregation in the intact protein, however, remained unclear.

96 The P1 and P2 regions control aggregation

97 To investigate how P1 and P2 affect α Syn aggregation, these regions were deleted individually (Δ P1
98 and Δ P2) or in tandem ($\Delta\Delta$) and the rate of aggregation monitored using thioflavin T (ThT)
99 fluorescence and compared with those of WT α Syn (Figure 2a-d, Extended Data Figure 1a-h and
100 Supplementary Table 1). The aggregates formed after 100 h were also imaged by negative stain
101 transmission electron microscopy (TEM) (Extended Data Figure 1) and fibril yield determined by
102 centrifugation (Supplementary Table 1). The results showed that decreasing the pH from 7.5 to 4.5
103 (mimicking cytosolic and lysosomal pH, respectively) in 200 mM NaCl accelerates the rate of
104 aggregation of WT α Syn, decreasing the lag-time ~6-fold and increasing the elongation rate ~10-fold
105 (Figure 2a, Supplementary Table 1) consistent with previous results^{44,45}. Aggregation of WT α Syn is
106 also affected by ionic strength⁴⁶, with assembly into amyloid occurring more rapidly at pH 4.5 at low
107 (20mM added NaCl) compared with high (200 mM added NaCl) ionic strength, while aggregation is
108 more rapid at pH 4.5 than pH 7.5 at both ionic strengths tested (Extended Data Figure 1a,b and
109 Supplementary Table 1).

110 Remarkably, deleting the 7-residue P1 sequence abolished aggregation (over 100 h) at pH 7.5 at low
111 and high ionic strength (Figure 2b, Extended Data Figure 1d, Supplementary Table 1). Deletion of P1
112 has a smaller effect at pH 4.5, with little effect at low ionic strength and a ~2-fold increase in the lag
113 time and a ~2-fold decrease in the elongation rate at high ionic strength (Figure 2b, Extended Data
114 Figure 1c, Supplementary Table 1). By contrast, deletion of P2 results in only modest effects under
115 all conditions studied (Figure 2c, Extended Data Figure 1e,f, Supplementary Table 1). Strikingly, the
116 $\Delta\Delta$ variant did not aggregate (over 100 h) at both pH values at high ionic strength, or at pH 7.5 at
117 low ionic strength, and the lag time of assembly was increased ~15-fold at pH 4.5 in low ionic
118 strength buffer (Figure 2d, Extended Data Figure 1g,h and Supplementary Table 1). This suggests a
119 dominant role for P1 in controlling the aggregation rate of this 140-residue IDP and shows that the
120 effects of P1 are synergistic with P2 at pH 4.5. $\Delta P1$ and $\Delta\Delta$ were also unable to elongate seeds
121 formed at pH 7.5 from WT α Syn, whilst $\Delta P2$ formed fibrils slowly (Extended Data Figure 2),
122 suggestive of a structural incompatibility of these sequences with fibril seeds formed from the WT
123 protein.

124 The importance of P1 and P2 in promoting aggregation was also assessed by measuring the
125 aggregation rate of disulfide cross-linked dimers of α Syn created by introducing Cys residues in P1
126 (V40C), P2 (V52C) or at the C-terminus (A140C). In the presence of 2 mM DTT, each variant formed
127 amyloid with kinetics similar to those of WT α Syn (Figure 3a-c, Supplementary Table 1). Dimerisation
128 (confirmed by SEC-MALS (see Methods)) prevented aggregation (for at least 140 h) for V40C (Figure
129 3a). However, such an effect was not observed for V52C or A140C (Figure 3b,c, Supplementary Table
130 1), supporting the finding that P1 is important for aggregation. The positional sensitivity of the
131 dimerisation site was not observed previously when α Syn was cross-linked by dityrosine formation
132 at Y39 and Y125, Y133 or Y136⁴⁷ suggesting a strict steric/positional sensitivity of inhibition. This
133 could act at the stage of dimer formation, or by the imposed dimerisation altering the structure of
134 seeds/oligomers formed later during assembly.

135 The presence of up to nine imperfect repetitive KTKEGV sequences in the N-terminal region of α Syn
136 raised the possibility that the effects of deleting P1 and/or P2 may result from changes in the spatial
137 organisation of the repeats (Figure 1b). To assess this possibility, a variant was constructed in which
138 a seven-residue sequence in a different location in the N-terminal region was deleted (residues 14-
139 20, denoted $\Delta C1$) (Figure 1b). $\Delta C1$ was designed to mimic the general features of P1 as closely as
140 possible i.e. the sequence deleted is of the same length and similar positioning between imperfect
141 repeats as P1. In contrast to the marked effects of deleting P1, $\Delta C1$ had no significant effect at pH
142 7.5 or pH 4.5 at high ionic strength, and even accelerated aggregation (decreasing the lag-time ~10-

143 fold) at pH 4.5 at low ionic strength (Extended Data Figure 3a-d, Supplementary Table 1). Fibrils were
144 also observed after 140 hours in all conditions as judged by negative stain EM and quantification of
145 soluble protein remaining (Extended Data Figure 3g, Supplementary Table 1). A second control
146 variant, named P1P2-GS, was also created in which the 7 residues in P1 and 13 residues in P2 were
147 replaced with alternating Gly-Ser sequences, 7 and 13 residues in length, respectively, preserving the
148 spacing of the imperfect repeats (Extended Data Figure 3a). At pH 7.5 P1P2-GS did not aggregate at
149 low or high ionic strength, similar to the behaviour of $\Delta\Delta$ (Extended Data Figure 3g,i, Supplementary
150 Table 1). At pH 4.5, aggregation did occur (Extended Data Figure 3f,i, but was significantly retarded
151 compared with WT α Syn (Supplementary Table 1). These data show that the effect of P1 and P2 on
152 aggregation is mainly sequence-specific and does not result from alterations in the length of the N-
153 terminal region or the spacing of the imperfect repeats.

154 **P1 and P2 make multiple intra-molecular contacts that promote amyloid formation**

155 To determine whether P1 and P2 affect the conformational properties of α Syn monomers that alter
156 their ability to assemble into amyloid, WT α Syn and $\Delta\Delta$ were examined using Paramagnetic
157 Relaxation Enhancement NMR (PRE NMR). This approach allows rare (0.5 – 5 % population) and
158 transient interactions to be investigated. Previous studies used NMR PREs to investigate the
159 conformational properties of WT α Syn at pH 2.5, 3.0, 6.0, 7.4 and 7.5 using protein concentrations
160 from 100 μ M to 650 μ M at 15 $^{\circ}$ C^{17,21,44,48-50}. The familial PD mutations (A30P, A53T)⁵¹ and β - and γ -
161 Syn⁵² have also been investigated using this approach. To determine how deletion of P1 and P2
162 affects the conformational properties of α Syn monomers, ¹⁵N WT α Syn containing a single Cys
163 introduced at positions 18 (α Syn A18C), 90 (α Syn A90C), or 140 (α Syn A140C) were expressed,
164 purified and their ¹H-¹⁵N HSQC spectra assigned at pH 4.5 (Methods). Each protein was then
165 covalently labelled with the paramagnetic spin label S-(1-oxyl-2,2,5,5-tetramethyl-2,5-dihydro-1H-
166 pyrrol-3-yl)methyl methanesulfonothioate (MTSL) and NMR PRE experiments performed to detect
167 transient intramolecular interactions. Control experiments confirmed that inter-molecular
168 interactions are not observed at the protein concentration used (see Methods). Under conditions
169 that promote rapid aggregation of WT α Syn (pH 4.5, 20 mM NaCl (low salt), Figure 4a) long range
170 intramolecular interactions between specific regions are observed for all three PRE probes (Figure
171 4b,d,f, Extended Data Figure 4). Specific intramolecular interactions between the N- and C-terminal
172 regions of the protein were observed, as exemplified by significant PRE effects when MTSL was
173 placed at residue 18 (Figure 4b), with a smaller reciprocal PRE effect from MTSL at residue 140 with
174 the N-terminal region (Figure 4f)), consistent with previous results at other pH values^{17,23,44}.
175 Significant contacts are also observed between NAC and the C-terminal region, consistent with

176 previous analyses at pH 2.5 and 3.0^{21,44}. Importantly, and by contrast with previous results²³,
177 significant PREs are observed between P1 (and some residues in P2) and residues near the N-
178 terminus (using α Syn A18, Figure 4b), as well as to NAC (using α Syn A90C, Figure 4d) and to C-
179 terminal regions (using α Syn A140C, Figure 4f). Previous meta-analysis of 11 PRE NMR studies also
180 showed evidence of the P1 and P2 regions as an interaction hub⁵³. Importantly, under conditions in
181 which aggregation is slowed (pH 4.5, 200 mM NaCl (high salt)) (Figure 4a), these intramolecular
182 interactions to P1/P2 (most markedly those involving PREs from residues 90 and 140) are decreased
183 in magnitude (compare Figure 4b,d,f with Figure 4c,e,g), consistent with electrostatic interactions,
184 possibly involving K45, E46, H49 or E57 in P2, or residues that juxtapose P1 (K32, K34, E35, K43)
185 and/or P2 (E61), being involved. The observation that weaker long range intra-molecular
186 interactions with P1/P2 results in slower aggregation kinetics suggests that these interactions are
187 important in defining the aggregation rate.

188 To determine how removing P1 and P2 affects the conformational properties of monomeric α Syn,
189 the PRE experiments were repeated under identical conditions (pH 4.5 at low and high ionic
190 strength) using $\Delta\Delta$ α Syn. These conditions result in slow (low salt) or no (high salt) fibril formation,
191 respectively (Figure 5a). The resulting PRE profiles (Figure 5b-g) show that the long range contacts
192 between the N- and C-terminal regions and the NAC and C-terminal region are mostly maintained in
193 $\Delta\Delta$, while contacts to P1/P2 were removed. Interestingly, while contacts between the N-terminal
194 region (residue 18) and NAC/C-terminal region and NAC (residue 90) and the N-/C-terminal regions
195 are similar in WT and $\Delta\Delta$ α Syn, those between the C-terminal region (residue 140) and the N-
196 terminal region are smaller in $\Delta\Delta$, indicative of a complex interplay of interactions that depends
197 intimately on the sequence and solution conditions. A further control experiment in which
198 intramolecular PREs were measured for P1P2-GS with MTSL at residue 90 showed a similar response,
199 with the long range intra-molecular PREs remaining in this construct and hints that the PRE effect to
200 the P1 and P2 regions observed for WT α Syn, is significantly reduced in P1P2-GS (Extended Data
201 Figure 5). Thus, removal of P1/P2 does not prevent compaction of the α Syn sequence, yet a
202 significant reduction in aggregation is observed, demonstrating the crucial importance of the P1/P2
203 sequences in determining the aggregation of α Syn.

204 **The roles of P1 and P2 in initiating intermolecular interactions**

205 At high protein concentrations (500 μ M), α Syn forms transient inter-molecular interactions, in which
206 residues 38-45 (corresponding closely to the P1 region (36-42)), make weak inter-chain interactions
207 with residues 124-140, at least at pH 6.0 at low ionic strength (10 mM MES, 0 M NaCl)⁵⁴. To
208 determine whether removal of P1 and P2 disrupts these inter-molecular interactions, 250 μ M ¹⁴N

209 α Syn was labelled with MTSL at residue 40 (V40C) or 129 (S129C) and incubated with 250 μ M 15 N WT
210 α Syn at pH 4.5 at low and high ionic strength. Intermolecular PREs (via R_2 relaxation experiments)
211 were then measured to identify inter-chain contacts (Extended Data Figure 6a,b). The results
212 showed that residue 40 (in the P1 region) makes intermolecular contacts primarily with residues in
213 the negatively charged C-terminal region of WT α Syn (Extended Data Figure 6b), in agreement with
214 published results⁵⁴. At high ionic strength (retarded aggregation), this effect is decreased, consistent
215 with these inter-molecular interactions being important in the early stages of aggregation (Extended
216 Data Figure 6b). Finally, intermolecular PREs were determined with MTSL at residue 129 (Extended
217 Data Figure 6c). These experiments showed a significant PRE from residue 129 to the P1 and P2
218 regions, as well as to the N-terminal ~20 residues in WT α Syn. Importantly, the latter interactions
219 are maintained in $\Delta\Delta$, whilst interactions with P1/P2 are no longer possible (Extended Data Figure
220 6c), showing that the inter-molecular contacts between the N- and C-termini are independent of the
221 presence of P1/P2. Together, the results reinforce the importance of the P1/P2 regions in driving
222 aggregation, not just because of their local insolubility and high aggregation-propensity, but also
223 because they determine the conformational properties of the monomeric IDP and formation of
224 transient intermolecular interactions with the C-terminal region, that define its ability to aggregate
225 into amyloid.

226 **P1 and P2 are drivers of aggregation *in vivo***

227 The effect of deleting P1 and P2 on α Syn aggregation *in vivo* was assessed by expressing WT α Syn,
228 Δ P1 or $\Delta\Delta$ fused C-terminally to YFP in *C. elegans* muscle cells³⁴. Figure 6a shows that WT α Syn::YFP
229 forms inclusions that are visible as foci in L4 larvae (Day 0). Foci increase in number as the animals
230 age, and the proteostasis network declines^{55,56}, reaching a plateau from Day 3 to Day 13 of
231 adulthood, as reported previously³⁴. In marked contrast, animals expressing Δ P1::YFP or $\Delta\Delta$::YFP
232 formed few, if any, visible aggregates throughout ageing (Figure 6a,b), even though the expression
233 levels of these proteins is higher than WT α Syn (Figure 6c). Notably, by contrast with WT α Syn::YFP,
234 the total number of Δ P1::YFP or $\Delta\Delta$::YFP foci did not increase during ageing, with few aggregates
235 observed even at Day 13 (Figure 6b). The percentage of immobile WT α Syn::YFP aggregates
236 increased ~4-fold from Day 7 to Day 13 of adulthood as measured by FRAP (Figure 6b). By
237 comparison, Δ P1 and $\Delta\Delta$ α Syn::YFP formed only few aggregates (1 to 2 foci) that were immobile
238 (Figure 6b). Even in aged worms motility remained similar to healthy N2 wild-type animals between
239 Days 0-3 (Figure 6d), with slightly reduced (2-fold) thrashing rates observed in $\Delta\Delta$::YFP and Δ P1::YFP
240 at Day 13 of adulthood (Figure 6d). In contrast, *C. elegans* expressing WT α Syn::YFP showed an age-
241 dependent decline of motility between Days 3 and 13 compared with N2 worms (Figure 6d). Thus,

242 deletion of P1 or both P1/P2 prevents both age-dependent aggregation of α Syn *in vivo* and
243 suppresses aggregation-induced proteotoxicity.

244 **The importance of P1/P2 in membrane remodelling**

245 As P1 and P2 are located in the membrane-binding N-terminal region of α Syn, we explored whether
246 P1/P2 also play a role in the function of α Syn in remodelling membrane vesicles^{35,57,58}. α Syn forms α -
247 helical structure in its N-terminal region (residues 1-97) upon membrane binding^{59,60} which
248 subsequently enhances aggregation of the protein into amyloid fibrils⁶¹. To determine whether $\Delta\Delta$ is
249 also able to adopt α -helical structure upon lipid binding, and whether this induces fibril formation,
250 the protein was incubated with liposomes prepared from 1,2-dimyristoyl-sn-glycero-3-phospho-L-
251 serine (DMPS), one of the major lipids in synaptic vesicles. The secondary structure of the protein
252 was then monitored using far UV CD. The resulting data (Figure 7a,b and Extended Data Figure 7a)
253 showed that $\Delta\Delta$ is able to bind to these vesicles, but adopts only 30% helical structure when
254 membrane bound, whilst 64 % helicity would be expected assuming similar helix formation to WT
255 α Syn. Lipid titration experiments revealed that the affinity of $\Delta\Delta$ for lipid is ~10-fold weaker than WT
256 α Syn ($K_D = 2.01 \pm 0.63 \mu\text{M}$ and $0.22 \pm 0.13 \mu\text{M}$ for $\Delta\Delta$ and WT α Syn, respectively) (Figure 7a,b,
257 Extended Data Figure 7b). The stoichiometry value, L, indicative of the total number of DMPS
258 molecules in the bilayer involved in binding one α Syn molecule, is similar for both proteins (49 and
259 33, respectively) (Figure 7a,b, Extended Data Figure 7b). P1P2-GS responds to DMPS liposomes
260 similarly to $\Delta\Delta$ (Figure 7c, Extended Data Figure 7b,c). Thus, the effect of P1/P2 is sequence specific
261 and does not result from changing the spacing of the imperfect repeats.

262 DMPS liposomes have also been shown to accelerate α Syn aggregation by promoting heterogeneous
263 primary nucleation⁶¹. To assess whether $\Delta\Delta$ α Syn is able to nucleate amyloid formation when bound
264 to these 160 nm diameter liposomes (Extended Data Figure 7d), the aggregation kinetics of WT
265 α Syn, $\Delta\Delta$ and P1P2-GS were monitored at different [DMPS]:[α Syn] molar ratios (Figure 7d-f).
266 Consistent with previous results, WT α Syn does not form amyloid in the absence of liposomes under
267 the conditions employed (20 mM sodium phosphate, pH 6.5)⁶¹, while an excess of lipid (60:1 [M:M])
268 also prevents aggregation by depleting the concentration of lipid-free monomer available for
269 elongation⁶¹. At an 8:1 [DMPS]:[α Syn] ratio, however, WT α Syn aggregates rapidly (Figure 7d), as
270 reported previously⁶¹. While $\Delta\Delta$ is able to nucleate amyloid formation at a ratio of 8:1 [M:M]
271 [DMPS]:[α Syn], the rate of aggregation is slowed significantly (lag times = 4.9 ± 0.3 h and 93.0 ± 2.6 h
272 for WT and $\Delta\Delta$, respectively) (Figure 7e, Supplementary Table 1), presumably because less helical
273 structure is formed in $\Delta\Delta$ in the lipid-bound state. Consistent with this P1P2-GS is able to aggregate,
274 but very slowly, when lipid bound (Figure 7c,f and Extended Data Figure 7b). Negative stain TEM of

275 sample at the endpoints of these incubations at 60:1 [DMPS]:[α Syn] [M:M] are shown in (Figures 7g-
276 i). Remarkably, while WT α Syn causes the coalescence of liposomes into long lipid tubes, as reported
277 previously³⁵, this is not observed upon incubation with $\Delta\Delta$ or P1P2-GS. Instead, incubation with
278 these proteins results in the formation of small, prefibrillar-like aggregates (Figure 7h,i (inset)) which
279 associate with the liposome surfaces and appear to cause liposome fission, releasing smaller
280 spherical liposomes (Figure 7h,i). Thus, in addition to controlling the aggregation of α Syn *in vitro* and
281 *in vivo*, P1/P2 affect the function of α Syn in re-modelling lipid vesicles.

282 Finally, membrane binding of WT, $\Delta\Delta$ and P1P2-GS were measured in residue-specific detail by
283 acquiring ¹⁵N-¹H HSQC NMR spectra of the proteins in the presence or absence of saturating
284 amounts (60:1 {M:M} [DMPS]:[α Syn]) of liposomes (Figure 8a-c). Due to the slow tumbling rates of
285 liposomes, resonances of residues that bind strongly are reduced in intensity, whilst those of lipid
286 free/weakly bound residues have higher intensity in the liposome-bound state⁶². Strikingly, these
287 data showed significant differences in the residues involved in lipid binding, with all but the C-
288 terminal ~20 residues binding strongly to lipid in $\Delta\Delta$, whilst a much smaller interface is formed for
289 WT α Syn. P1P2-GS exhibited intermediate behaviour, suggesting that both the sequence and the
290 relative position of P1 and P2 play a role in lipid binding (Figure 8d). Thus, the P1/P2-regions control
291 the lipid-binding properties of distal regions of the α Syn sequence, structure in the lipid-bound state
292 and perturb membrane remodelling, without preventing binding to DMPS liposomes.

293

294 Discussion

295 The P1 sequence is a 'master-controller' of α Syn aggregation

296 We have identified a sequence in the N-terminal region of α Syn (residues 36-42 (P1)) that plays a
297 key role in determining the ability of the protein to form amyloid fibrils *in vitro* and *in vivo*.
298 Remarkably, we show that the seven residue P1 segment is specifically required for aggregation,
299 with its deletion preventing aggregation *in vitro* at neutral pH and in bodywall muscle cells of *C.*
300 *elegans*, despite the protein retaining the crucial NAC region¹². By performing aggregation assays
301 and NMR PRE experiments under conditions which either favour (pH 4.5 (lysosomal conditions), low
302 ionic strength) or deter (pH 7.5 (cytosolic), high ionic strength) (Supplementary
303 Table 1) amyloid growth, we have been able to correlate changes in monomer conformation (e.g.
304 changes in the intra-molecular long-range interactions for P1/P2 measured by NMR-PRE at pH 4.5)
305 induced by sequence changes in the P1/P2 region with aggregation propensity. Based on these
306 observations we define the P1 region as a 'master-controller' of α Syn aggregation, in that this region
307 controls α Syn self-assembly, synergistically with the P2 (Pre-NAC) region³² under some conditions
308 (specifically at low pH values that mimic the lysosomal environment, relevant for α Syn *in vivo*⁶³).
309 These regions exert their control by fine-tuning intra- and inter-molecular contacts both locally
310 within the N-terminal region, and with the distal NAC and C-terminal regions, yielding a
311 conformational ensemble that is either aggregation-prone (retaining P1 or P1/P2) or protected from
312 aggregation (P1 or P1/P2 deleted or substituted with Gly-Ser), presumably via
313 exposure/sequestration of the crucial^{12,22,23} NAC region. The precise molecular mechanism by which
314 this is accomplished, including the relative importance of each residue in P1 in defining the protein's
315 behaviour, remain to be elucidated. Deletion of P1/P2 could also affect the structure and
316 aggregation-competence of oligomers formed later during aggregation. Whatever the precise
317 mechanism of action, the sensitivity of aggregation to pH and ionic strength suggests that P1/P2
318 control α Syn aggregation by a delicate balance of hydrophobicity and charge, such that aggregation
319 becomes highly sensitive to the solution conditions. This may rationalise why P1/P2 interactions
320 eluded detection in previous studies at pH values below^{21,44,48} or above^{17,44,48-50} pH 4.5. Thus, while
321 NAC is necessary and sufficient for α Syn aggregation¹², the ability to prevent aggregation at pH 7.5
322 by removal or substitution of a single, specific, 7-residue sequence provides a striking demonstration
323 of the crucial effect of flanking regions in amyloid formation.

324 The importance of flanking region(s) has been demonstrated for other aggregation-prone proteins,
325 including the P17 region in exon 1 of huntingtin^{25,26,28}, the N-terminal region (residue 11-16) of

326 amyloid β ($A\beta_{40}$)⁶⁴, residues 306-311 in tau⁶⁵, the aggregation prone motifs 14–22, 53–58, and 69–72
327 in the N-terminal region of Apo-I²⁴ and the N-terminal six amino acids of β_2 -microglobulin⁶⁶. At
328 longer timescales, or under more favourable conditions for aggregation (e.g. at pH 4.5 and low ionic
329 strength (Extended Data Figure 1g) or at pH 6.5 in the presence of DMPS liposomes (Figure 7e)), $\Delta\Delta$
330 is able to form amyloid, highlighting the crucial role of the transient intra- and inter-molecular
331 interactions made by the N-terminal region of α Syn in imposing kinetic control on the
332 thermodynamically favourable process of amyloid formation.

333 Our discovery that P1 and P2 are also required for the function of α Syn in vesicle remodelling adds
334 to the growing evidence that the N-terminal region of α Syn is important for both its physiological
335 function and its disease aetiology^{57,67}. Notably, P2 encompasses six of the seven early onset familial
336 PD mutations⁶⁸ (Figure 1b). This region also forms the protofilament interface in some^{13,14,33}, but not
337 all¹³, structures of α Syn fibrils formed *in vitro*, and this region can form amyloid in isolation³². Hoyer
338 and colleagues also showed that the aggregation of α Syn can be inhibited *in vitro* and *in vivo* by the
339 binding of a β -wrapin^{41,43} to residues 37-54, which encompasses both P1 and P2, with the NMR
340 structure of the complex revealing β -hairpin formation involving residues ³⁷VLYVGSK⁴³ and
341 ⁴⁸VVHGVAT⁵⁴ of α Syn⁴¹. Engineering an intramolecular disulphide bond between residues 41 and 48
342 has also been shown to inhibit α Syn aggregation in the absence of β -hairpin formation⁴²,
343 presumably because this perturbs the structure around P1 and P2 that we show here to be vital for
344 fibril formation. Mutation of Y39 to Ala also prevents aggregation and Y39 has been shown to be
345 responsible (together with F94) for binding small molecules able to retard aggregation⁶². Finally, a
346 cyclised peptide of residue 36-55 has been shown to adopt a β -hairpin structure that self-assembles
347 into cytotoxic oligomers, the authors suggesting that this region, rather than NAC, nucleates
348 oligomer formation¹¹. Together, the data presented here highlight the vital importance of P1 and P2
349 in controlling α Syn aggregation, demonstrating that aggregation is not initiated by the NAC region
350 alone. Using a *C. elegans* model expressing α Syn in the bodywall muscles, deletion of P1 or both P1
351 and P2 suppressed age-dependent α Syn inclusion body formation as well as the associated toxicity,
352 resulting in animals with improved health-span, even at advanced age. Displacing the interactions
353 made by P1 and/or P2 may thus pave the way to routes to control α Syn aggregation using small
354 molecules or other reagents that target these sites.

355 **Frustration between aggregation and function**

356 Given that deletion of P1 and P2 neutralises the deleterious effects of NAC on α Syn aggregation,
357 why is the sequence of these regions retained by evolution? While the physiological function(s) of
358 α Syn remain unclear, stabilisation, sequestration, and fusion of pre-synaptic vesicles are thought to

359 be involved in its repertoire of functions^{36,57,69}. Distinct membrane binding sites within the N-
360 terminal region involving residues 1-25 and 65-97 have been proposed to play a critical role in
361 tethering vesicles prior to membrane fusion^{35,36}. Here we show that deleting part of the 'passive'
362 linker region between these two sites (residues 36-57 in P1/P2) prevents the function of α Syn in
363 membrane remodelling, generating liposome morphologies that are distinct from the large fused
364 tubular structures formed by the WT protein (Figure 7g-i). Together with their effects on
365 aggregation, the results demonstrate the frustration between function and aggregation in this IDP,
366 with the presence of the P1/P2 region being required for function, whilst simultaneously generating
367 a sequence that enhances amyloid assembly. Such a delicate balance rationalises why single point
368 mutations such as A53T, E46K and others⁶⁸, enhance Parkinson's disease onset by simultaneously
369 causing loss-of-function and gain-of-toxic function activities. For an IDP such as α Syn the aggregation
370 propensity of such aggregation-prone, yet functionally important regions, cannot be protected by
371 the framework of a folded tertiary structure, making such sequences especially prone to be the
372 causative agents of disease. Indeed 17 of the 48 currently known human amyloidogenic proteins are
373 IDPs or contain intrinsically disordered regions³. Such sequences enable dangerous liaisons since
374 their intrinsic amyloid potential is exposed, unabridged by the protection of a native structure.
375 Nonetheless, the presence of such newly discovered and characterised 'master-controllers' of
376 aggregation within the α Syn sequence offers exciting potentials to control amyloid formation by
377 binding small molecules, chaperones, biologics or other agents to these regions. Given the fine
378 balance of weak intra- and inter-molecular interactions that control the early stages of aggregation
379 into amyloid, minor alterations in the shape of the interaction energy landscape could disable
380 aggregation without significantly perturbing function. Further experiments will be needed to identify
381 whether other IDPs contain 'master-controllers' of aggregation, to identify the role of each of the
382 seven amino acids in P1 in encoding the ability to control α Syn aggregation and function and to
383 clarify the molecular mechanism of fibril growth inhibition by P1 in more detail.

384

385 **Acknowledgments**

386 We thank members of our research groups for helpful discussions throughout this work. We also
387 thank Theo Karamanos for helpful advice about NMR PRE data analysis, Ellen Nollen (University of
388 Groningen) for the kind gift of the plasmid encoding YFP- α Syn, Leon Willis for help with SEC-MALS
389 analysis, Bob Schiffrin for his help with the K_d fitting and the mass spectrometry facility for help with
390 characterisation of all purified proteins. SER acknowledges funding from the European Research
391 Council under the European Union's Seventh Framework Programme FP7.2007-2013/Grant
392 agreement number 322408 and Wellcome Trust (204963). CPAD was supported by BBSRC

393 (BB/K02101X/1) and by the ERC (322408), SCG by BBSRC (BB/M011151/1), RMM by Wellcome Trust
394 (204963) and SMU by the Wellcome Trust (215062/Z/18/Z). PvOH is also funded N3CR grant
395 (NC/P001203/1). We thank the Wellcome Trust (094232) and University of Leeds for the purchase of
396 the Chiroscan CD spectrometer, the electron microscopes and NMR instrumentation.

397 **Author Contributions**

398 CPAD and SMU prepared samples, designed and performed fluorescence, NMR experiments, EM and
399 other biochemical studies, JM, SCG and PvOH performed the experiments with *C. elegans*. CPAD,
400 SMU and GNK performed CD experiments. RMM performed NMR assignment and assisted with NMR
401 data analysis and interpretation. SER and DJB developed the ideas and supervised the work. All
402 authors contributed to the preparation of the manuscript.

403 **Competing interests**

404 No authors have competing interests.

405

406

407 **References**

- 408 1. Iwai, A., Masliah, E., Yoshimoto, M., Ge, N.F., Flanagan, L. *et al.* The precursor protein of
409 non-a-beta component of Alzheimers-disease amyloid is a presynaptic protein of the central-
410 nervous-system. *Neuron* **14**, 467-475 (1995).
- 411 2. Dettmer, U., Selkoe, D. & Bartels, T. New insights into cellular alpha-synuclein homeostasis
412 in health and disease. *Curr. Opin. Neurobiol.* **36**, 15-22 (2016).
- 413 3. Iadanza, M.G., Jackson, M.P., Hewitt, E.W., Ranson, N.A. & Radford, S.E. A new era for
414 understanding amyloid structures and disease. *Nat. Rev. Mol. Cell Biol.* (2018).
- 415 4. Tysnes, O.-B. & Storstein, A. Epidemiology of Parkinson's disease. *J. Neural. Transm.* **124**,
416 901-905 (2017).
- 417 5. Weinreb, P.H., Zhen, W., Poon, A.W., Conway, K.A. & Lansbury, P.T. NACP, a protein
418 implicated in Alzheimer's disease and learning, is natively unfolded. *Biochemistry* **35**, 13709-
419 13715 (1996).
- 420 6. Theillet, F.-X., Binolfi, A., Bekei, B., Martorana, A., Rose, H.M. *et al.* Structural disorder of
421 monomeric α -synuclein persists in mammalian cells. *Nature* **530**, 45 (2016).
- 422 7. Fusco, G., Chen, S.W., Williamson, P.T.F., Cascella, R., Perni, M. *et al.* Structural basis of
423 membrane disruption and cellular toxicity by α -synuclein oligomers. *Science* **358**, 1440-1443
424 (2017).
- 425 8. Chen, S.W., Drakulic, S., Deas, E., Ouberai, M., Aprile, F.A. *et al.* Structural characterization of
426 toxic oligomers that are kinetically trapped during alpha-synuclein fibril formation. *Proc.*
427 *Natl. Acad. Sci. U. S. A.* **112**, E1994-2003 (2015).
- 428 9. Peelaerts, W., Bousset, L., Van der Perren, A., Moskalyuk, A., Pulizzi, R. *et al.* Alpha-synuclein
429 strains cause distinct synucleinopathies after local and systemic administration. *Nature* **522**,
430 340+ (2015).
- 431 10. Bartels, T., Ahlstrom, L.S., Leftin, A., Kamp, F., Haass, C. *et al.* The N-terminus of the
432 intrinsically disordered protein α -synuclein triggers membrane binding and helix folding.
433 *Biophys. J.* **99**, 2116-2124 (2010).
- 434 11. Salvesson, P.J., Spencer, R.K. & Nowick, J.S. X-ray crystallographic structure of oligomers
435 formed by a toxic β -hairpin derived from α -synuclein: Trimers and higher-order oligomers. *J.*
436 *Am. Chem. Soc.* **138**, 4458-4467 (2016).
- 437 12. Giasson, B.I., Murray, I.V., Trojanowski, J.Q. & Lee, V.M. A hydrophobic stretch of 12 amino
438 acid residues in the middle of alpha-synuclein is essential for filament assembly. *J. Biol.*
439 *Chem.* **276**, 2380-6 (2001).
- 440 13. Li, B., Ge, P., Murray, K.A., Sheth, P., Zhang, M. *et al.* Cryo-em of full-length α -synuclein
441 reveals fibril polymorphs with a common structural kernel. *Nat. Commun.* **9**, 3609 (2018).
- 442 14. Guerrero-Ferreira, R., Taylor, N.M.I., Mona, D., Ringler, P., Lauer, M.E. *et al.* Cryo-EM
443 structure of alpha-synuclein fibrils. *Elife* **7**(2018).
- 444 15. Tuttle, M.D., Comellas, G., Nieuwkoop, A.J., Covell, D.J., Berthold, D.A. *et al.* Solid-state NMR
445 structure of a pathogenic fibril of full-length human alpha-synuclein. *Nat. Struct. Mol. Biol.*
446 **23**, 409-15 (2016).
- 447 16. Allison, J.R., Varnai, P., Dobson, C.M. & Vendruscolo, M. Determination of the free energy
448 landscape of alpha-synuclein using spin label nuclear magnetic resonance measurements. *J.*
449 *Am. Chem. Soc.* **131**, 18314-18326 (2009).

- 450 17. Bertocini, C.W., Jung, Y.S., Fernandez, C.O., Hoyer, W., Griesinger, C. *et al.* Release of long-
451 range tertiary interactions potentiates aggregation of natively unstructured alpha-synuclein.
452 *Proc. Natl. Acad. Sci. U. S. A.* **102**, 1430-1435 (2005).
- 453 18. Rao, J.N., Jao, C.C., Hegde, B.G., Langen, R. & Ulmer, T.S. A combinatorial nmr and EPR
454 approach for evaluating the structural ensemble of partially folded proteins. *J. Am. Chem.*
455 *Soc.* **132**, 8657-8668 (2010).
- 456 19. Phillips, A.S., Gomes, A.F., Kalapothakis, J.M., Gillam, J.E., Gasparavicius, J. *et al.*
457 Conformational dynamics of α -synuclein: Insights from mass spectrometry. *Analyst* **140**,
458 3070-3081 (2015).
- 459 20. Uversky, V.N., Li, J. & Fink, A.L. Evidence for a partially folded intermediate in alpha-
460 synuclein fibril formation. *J. Biol. Chem.* **276**, 10737-10744 (2001).
- 461 21. Wu, K.P., Weinstock, D.S., Narayanan, C., Levy, R.M. & Baum, J. Structural reorganization of
462 alpha-synuclein at low pH observed by NMR and REMD simulations. *J. Mol. Biol.* **391**, 784-
463 796 (2009).
- 464 22. Hoyer, W., Cherny, D., Subramaniam, V. & Jovin, T.M. Impact of the acidic C-terminal region
465 comprising amino acids 109– 140 on α -synuclein aggregation in vitro. *Biochemistry* **43**,
466 16233-16242 (2004).
- 467 23. Stephens, A.D., Zacharopoulou, M. & Kaminski Schierle, G.S. The cellular environment affects
468 monomeric α -synuclein structure. *Trends Biochem. Sci.* (2018).
- 469 24. Das, M., Mei, X., Jayaraman, S., Atkinson, D. & Gursky, O. Amyloidogenic mutations in
470 human apolipoprotein A-I are not necessarily destabilizing—a common mechanism of
471 apolipoprotein A-I misfolding in familial amyloidosis and atherosclerosis. *The FEBS journal*
472 **281**, 2525-2542 (2014).
- 473 25. Hoop, C.L., Lin, H.-K., Kar, K., Hou, Z., Poirier, M.A. *et al.* Polyglutamine amyloid core
474 boundaries and flanking domain dynamics in huntingtin fragment fibrils determined by solid-
475 state nuclear magnetic resonance. *Biochemistry* **53**, 6653-6666 (2014).
- 476 26. Bugg, C.W., Isas, J.M., Fischer, T., Patterson, P.H. & Langen, R. Structural features and
477 domain organization of huntingtin fibrils. *J. Biol. Chem.* **287**, 31739-31746 (2012).
- 478 27. Colvin, M.T., Silvers, R., Ni, Q.Z., Can, T.V., Sergeev, I. *et al.* Atomic resolution structure of
479 monomeric β 42 amyloid fibrils. *J. Am. Chem. Soc.* **138**, 9663-9674 (2016).
- 480 28. Lucato, C.M., Lupton, C.J., Halls, M.L. & Ellisdon, A.M. Amyloidogenicity at a distance: How
481 distal protein regions modulate aggregation in disease. *J. Mol. Biol.* **429**, 1289-1304 (2017).
- 482 29. Crowther, R.A., Jakes, R., Spillantini, M.G. & Goedert, M. Synthetic filaments assembled from
483 C-terminally truncated α -synuclein. *FEBS Lett.* **436**, 309-312 (1998).
- 484 30. Kessler, J.C., Rochet, J.-C. & Lansbury, P.T. The N-terminal repeat domain of α -synuclein
485 inhibits β -sheet and amyloid fibril formation. *Biochemistry* **42**, 672-678 (2003).
- 486 31. Izawa, Y., Tateno, H., Kameda, H., Hirakawa, K., Hato, K. *et al.* Role of C-terminal negative
487 charges and tyrosine residues in fibril formation of alpha-synuclein. *Brain and Behavior* **2**,
488 595-605 (2012).
- 489 32. Rodriguez, J.A., Ivanova, M.I., Sawaya, M.R., Cascio, D., Reyes, F.E. *et al.* Structure of the
490 toxic core of alpha-synuclein from invisible crystals. *Nature* **525**, 486-90 (2015).
- 491 33. Li, Y., Zhao, C., Luo, F., Liu, Z., Gui, X. *et al.* Amyloid fibril structure of α -synuclein determined
492 by cryo-electron microscopy. *Cell Res.* **28**, 897 (2018).
- 493 34. Van Ham, T.J., Thijssen, K.L., Breitling, R., Hofstra, R.M., Plasterk, R.H. *et al.* C. Elegans model

- 494 identifies genetic modifiers of α -synuclein inclusion formation during aging. *PLoS genetics* **4**,
495 e1000027 (2008).
- 496 35. Fusco, G., Pape, T., Stephens, A.D., Mahou, P., Costa, A.R. *et al.* Structural basis of synaptic
497 vesicle assembly promoted by alpha-synuclein. *Nat. Commun.* **7**(2016).
- 498 36. Lautenschläger, J., Stephens, A.D., Fusco, G., Ströhl, F., Curry, N. *et al.* C-terminal calcium
499 binding of α -synuclein modulates synaptic vesicle interaction. *Nat. Commun.* **9**, 712 (2018).
- 500 37. Tartaglia, G.G. & Vendruscolo, M. The Zyggregator method for predicting protein
501 aggregation propensities. *Chem. Soc. Rev.* **37**, 1395-1401 (2008).
- 502 38. Sormanni, P., Aprile, F.A. & Vendruscolo, M. The camsol method of rational design of protein
503 mutants with enhanced solubility. *J. Mol. Biol.* **427**, 478-490 (2015).
- 504 39. Thompson, M.J., Sievers, S.A., Karanicolas, J., Ivanova, M.I., Baker, D. *et al.* The 3D profile
505 method for identifying fibril-forming segments of proteins. *Proc. Natl. Acad. Sci. U. S. A.* **103**,
506 4074-4078 (2006).
- 507 40. Terada, M., Suzuki, G., Nonaka, T., Kametani, F., Tamaoka, A. *et al.* The effect of truncation
508 on prion-like properties of α -synuclein. *J. Biol. Chem.* **293**, 13910-13920 (2018).
- 509 41. Mirecka, E.A., Shaykhalishahi, H., Gauhar, A., Akgul, S., Lecher, J. *et al.* Sequestration of a
510 beta-hairpin for control of alpha-synuclein aggregation. *Angew Chem Int Ed Engl* **53**, 4227-30
511 (2014).
- 512 42. Shaykhalishahi, H., Gauhar, A., Wordehoff, M.M., Gruning, C.S., Klein, A.N. *et al.* Contact
513 between the beta1 and beta2 segments of alpha-synuclein that inhibits amyloid formation.
514 *Angew Chem Int Ed Engl* **54**, 8837-40 (2015).
- 515 43. Agerschou, E.D., Saridakis, T., Flagmeier, P., Galvagnion, C., Komnig, D. *et al.* An engineered
516 monomer binding-protein for α -synuclein efficiently inhibits the proliferation of amyloid
517 fibrils. *Elife* **8**, e46112 (2019).
- 518 44. Cho, M.K., Nodet, G., Kim, H.Y., Jensen, M.R., Bernado, P. *et al.* Structural characterization of
519 α -synuclein in an aggregation prone state. *Protein Sci.* **18**, 1840-1846 (2009).
- 520 45. Buell, A.K., Galvagnion, C., Gaspar, R., Sparr, E., Vendruscolo, M. *et al.* Solution conditions
521 determine the relative importance of nucleation and growth processes in α -synuclein
522 aggregation. *Proc. Natl. Acad. Sci.* **111**, 7671-7676 (2014).
- 523 46. Hoyer, W., Antony, T., Cherny, D., Heim, G., Jovin, T.M. *et al.* Dependence of α -synuclein
524 aggregate morphology on solution conditions. *J. Mol. Biol.* **322**, 383-393 (2002).
- 525 47. Wördehoff, M.M., Shaykhalishahi, H., Groß, L., Gremer, L., Stoldt, M. *et al.* Opposed effects
526 of dityrosine formation in soluble and aggregated α -synuclein on fibril growth. *J. Mol. Biol.*
527 **429**, 3018-3030 (2017).
- 528 48. Wu, K.-P. & Baum, J. Detection of transient interchain interactions in the intrinsically
529 disordered protein α -synuclein by nmr paramagnetic relaxation enhancement. *J. Am. Chem.*
530 *Soc.* **132**, 5546-5547 (2010).
- 531 49. Dedmon, M.M., Lindorff-Larsen, K., Christodoulou, J., Vendruscolo, M. & Dobson, C.M.
532 Mapping long-range interactions in α -synuclein using spin-label NMR and ensemble
533 molecular dynamics simulations. *J. Am. Chem. Soc.* **127**, 476-477 (2005).
- 534 50. Wu, K.-P., Kim, S., Fela, D.A. & Baum, J. Characterization of conformational and dynamic
535 properties of natively unfolded human and mouse α -synuclein ensembles by NMR:
536 Implication for aggregation. *J. Mol. Biol.* **378**, 1104-1115 (2008).
- 537 51. Bertocini, C.W., Fernandez, C.O., Griesinger, C., Jovin, T.M. & Zweckstetter, M. Familial

- 538 mutants of α -synuclein with increased neurotoxicity have a destabilized conformation. *J.*
539 *Biol. Chem.* **280**, 30649-30652 (2005).
- 540 52. Sung, Y.-h. & Eliezer, D. Residual structure, backbone dynamics, and interactions within the
541 synuclein family. *J. Mol. Biol.* **372**, 689 (2007).
- 542 53. Esteban-Martín, S., Silvestre-Ryan, J., Bertocini, C.W. & Salvatella, X. Identification of fibril-
543 like tertiary contacts in soluble monomeric α -synuclein. *Biophys. J.* **105**, 1192-1198 (2013).
- 544 54. Janowska, M.K., Wu, K.-P. & Baum, J. Unveiling transient protein-protein interactions that
545 modulate inhibition of alpha-synuclein aggregation by beta-synuclein, a pre-synaptic protein
546 that co-localizes with alpha-synuclein. *Scientific reports* **5**, 15164-15164 (2015).
- 547 55. Ben-Zvi, A., Miller, E.A. & Morimoto, R.I. Collapse of proteostasis represents an early
548 molecular event in *Caenorhabditis elegans* aging. *Proc. Natl. Acad. Sci.* **106**, 14914-14919
549 (2009).
- 550 56. Labbadia, J. & Morimoto, R.I. Repression of the heat shock response is a programmed event
551 at the onset of reproduction. *Mol. Cell* **59**, 639-650 (2015).
- 552 57. Diao, J., Burré, J., Vivona, S., Cipriano, D.J., Sharma, M. *et al.* Native α -synuclein induces
553 clustering of synaptic-vesicle mimics via binding to phospholipids and synaptobrevin-
554 2/VAMP2. *Elife* **2**, e00592 (2013).
- 555 58. Bodner, C.R., Dobson, C.M. & Bax, A. Multiple tight phospholipid-binding modes of α -
556 synuclein revealed by solution NMR spectroscopy. *J. Mol. Biol.* **390**, 775-790 (2009).
- 557 59. Fusco, G., De Simone, A., Gopinath, T., Vostrikov, V., Vendruscolo, M. *et al.* Direct
558 observation of the three regions in α -synuclein that determine its membrane-bound
559 behaviour. *Nat. Commun.* **5**, 3827 (2014).
- 560 60. Jao, C.C., Hegde, B.G., Chen, J., Haworth, I.S. & Langen, R. Structure of membrane-bound α -
561 synuclein from site-directed spin labeling and computational refinement. *Proc. Natl. Acad.*
562 *Sci.* **105**, 19666-19671 (2008).
- 563 61. Galvagnion, C., Buell, A.K., Meisl, G., Michaels, T.C., Vendruscolo, M. *et al.* Lipid vesicles
564 trigger alpha-synuclein aggregation by stimulating primary nucleation. *Nat. Chem. Biol.* **11**,
565 229-34 (2015).
- 566 62. Fonseca-Ornelas, L., Eisbach, S.E., Paulat, M., Giller, K., Fernández, C.O. *et al.* Small molecule-
567 mediated stabilization of vesicle-associated helical α -synuclein inhibits pathogenic
568 misfolding and aggregation. *Nat. Commun.* **5**, 5857 (2014).
- 569 63. Jackson, M.P. & Hewitt, E.W. Cellular proteostasis: Degradation of misfolded proteins by
570 lysosomes. *Essays Biochem.* **60**, 173-180 (2016).
- 571 64. Brännström, K., Öhman, A., Nilsson, L., Pihl, M., Sandblad, L. *et al.* The N-terminal region of
572 amyloid β controls the aggregation rate and fibril stability at low pH through a gain of
573 function mechanism. *J. Am. Chem. Soc.* **136**, 10956-10964 (2014).
- 574 65. Chen, D., Drombosky, K.W., Hou, Z., Sari, L., Kashmer, O.M. *et al.* Tau local structure shields
575 an amyloid-forming motif and controls aggregation propensity. *Nat. Commun.* **10**, 2493
576 (2019).
- 577 66. Esposito, G., Michelutti, R., Verdone, G., Viglino, P., Hernandez, H. *et al.* Removal of the N-
578 terminal hexapeptide from human β 2-microglobulin facilitates protein aggregation and fibril
579 formation. *Protein Sci.* **9**, 831-845 (2000).
- 580 67. Goedert, M. Alpha-synuclein and neurodegenerative diseases. *Nat. Rev. Neurosci.* **2**, 492
581 (2001).

- 582 68. Mehra, S., Sahay, S. & Maji, S.K. α -synuclein misfolding and aggregation: Implications in
583 Parkinson's disease pathogenesis. *Biochimica et Biophysica Acta (BBA)-Proteins and*
584 *Proteomics* (2019).
- 585 69. Cabin, D.E., Shimazu, K., Murphy, D., Cole, N.B., Gottschalk, W. *et al.* Synaptic vesicle
586 depletion correlates with attenuated synaptic responses to prolonged repetitive stimulation
587 in mice lacking α -synuclein. *J. Neurosci.* **22**, 8797-8807 (2002).
588

589 **Figure Legends**

590 **Figure 1. Aggregation and solubility profiles of α Syn.** a) The sequence of human α Syn. The N-
591 terminal region (1-60), NAC region (61-95) and C-terminal region (96-140) are coloured in blue, pink,
592 and red, respectively. The C1 and P1/P2 regions shown in (b) are coloured pale grey and dark grey
593 respectively. The imperfect KTKEGV repeats are underlined in blue. b) Regions of α Syn highlighting
594 the imperfect KTKEGV repeats in the N-terminal region (light blue), the positions of the seven
595 familial PD mutants, and the P1, P2 and C1 control sequence highlighted as in (a). c), d) and e)
596 Zyggregator³⁷, Camsol³⁸ and ZipperDB³⁹ profiles for the α Syn sequence, respectively. Red bars
597 indicate aggregation-prone/low solubility regions. Yellow bars indicate residues with a higher than
598 average aggregation propensity/low solubility, but which do not meet the threshold. Red dashed
599 lines indicate the low solubility/high aggregation propensity threshold, while green dashed lines
600 show threshold values for high solubility/low aggregation propensity. For Zipper DB, the yellow
601 dashed line shows the threshold value of residues with a high probability of β -zipper formation³⁹.
602 Data for graphs in c-e are available as Source Data.

603

604 **Figure 2. The kinetics of aggregation of WT α Syn and P1/P2 deletion variants.** a-d The
605 aggregation kinetics of 100 μ M WT α Syn (a); Δ P1 (b); Δ P2 (c) or $\Delta\Delta$ variants (d). Dark and light
606 colours denote incubations carried out at pH 7.5 (20 mM Tris HCl, 200 mM NaCl, pH 7.5) or pH 4.5
607 (20 mM sodium acetate, 200 mM NaCl, pH 4.5), respectively. All experiments were carried out at 37
608 °C with agitation at 600 rpm and measured in at least triplicate. Lag times and elongation rates were
609 determined for every single curve using OriginPro (see Methods), means and s.d. are listed in
610 [Supplementary Table 1](#). The fibril yield under each condition, determined by SDS PAGE subsequent
611 to centrifugation (see Methods), is shown in [Supplementary Table 1](#). Data for all graphs are available
612 as Source Data.

613

614 **Figure 3. ThT fluorescence assays of disulfide locked α Syn dimers.** a-c Aggregation kinetics
615 and negative stain TEM images of endpoint (140 h) aggregates of 100 μ M V40C (a), V52C (b) or
616 A140C (c) monomers or dimers. Incubations of monomeric or disulfide locked dimers of α Syn are
617 shown in light and dark red, respectively. Aggregation kinetics of WT α Syn are shown in blue. The
618 same data for the WT α Syn are shown overlaid for all three variants. All experiments were measured
619 in at least triplicate. TEMs with light border show end point images of reduced samples and dark
620 borders show end point images of disulfide bonded dimers. Each image was collected from a

621 representative sample for each condition., All assays were carried out in 20 mM sodium acetate
622 buffer, containing 200 mM NaCl, pH 4.5 (including 2 mM DTT for reduced samples), 37 °C with
623 agitation at 600 rpm. Data for all ThT graphs are available as Source Data.

624

625 **Figure 4. Intramolecular PRE experiments for WT α Syn.** a) Aggregation kinetics (note the short
626 timescale depicted) of WT α Syn (100 μ M in 20 mM sodium acetate, pH 4.5, at low (20 mM added
627 NaCl) or high (200 mM added NaCl) ionic strength at 37 °C). b-g Intramolecular PRE intensity ratios of
628 amide protons (paramagnetic/diamagnetic) for WT α Syn variants with MTSL spin labels at A18C
629 (b,c), A90C (d,e) or A140C (f,g) at low (b,d,f) or high (c,e,g) ionic strengths, 15 °C , as indicated. Blue,
630 pink and red bars show intensity ratios for the N-terminal, NAC and C-terminal regions, respectively.
631 Dark blue bars highlighted in grey point out the position of the P1/P2 region. Schematics are shown
632 above each plot with a consistent colour scheme. The location of spin labels are denoted by a yellow
633 circle. Grey panels highlight the location of the P1/P2 regions. Data for all graphs are available as
634 Source Data.

635

636 **Figure 5. Intramolecular PRE experiments for $\Delta\Delta$ α Syn.** a) Aggregation kinetics (note different
637 timescale compared with [Extended Data Figure 1](#)) of $\Delta\Delta$ and WT α Syn (100 μ M in 20 mM sodium
638 acetate, pH 4.5, 37 °C at low (20 mM added NaCl) or high (200 mM added NaCl) ionic strength). b-g)
639 Intramolecular PRE intensity ratios of amide protons (paramagnetic/diamagnetic) for variants with
640 MTSL spin labels at A18C (b,c), A90C (d,e) or A140C (f,g) at low (b,d,f) or high (c,e,g) ionic strengths,
641 at 15 °C, as indicated. Data for all graphs are available as Source Data.

642

643 **Figure 6. Deletion of P1 or P1/P2 in *C. elegans* expressing α Syn::YFP suppresses**
644 **aggregation and proteotoxicity.** a) Confocal microscopy images showing the head region of
645 transgenic *C. elegans* expressing WT α Syn, $\Delta\Delta$ or Δ P1 tagged C-terminally to YFP in the bodywall
646 muscle during ageing (Day 0 to Day 13 of adulthood). Scale bar, 10 μ m. b) Number of mobile and
647 immobile inclusions larger than $\sim 2 \mu\text{m}^2$ per animal between the tip of the nose and pharyngeal bulb
648 during ageing determined using FRAP. Data shown are the mean and s.e.m. for three independent
649 experiments (biological replicates); in each experiment, 10 worms ($n = 10$) were assessed for each
650 time point. ($n=10$ worms). Blue stars indicate significance between the number of mobile aggregates
651 of animals expressing WT α Syn or the variants Δ P1 or $\Delta\Delta$. Red stars indicate significance between
652 the number of immobile aggregates exhibited in animals expressing WT α Syn compared with

653 mutant animals. *P<0.05; **P<0.01; ***P<0.001; ****P<0.0001. A one-sided Student's t test was
654 used in all cases. c) Western blot analysis of protein extracts isolated from N2, WT α Syn::YFP,
655 Δ P1::YFP and $\Delta\Delta$::YFP animals using an anti- α Syn antibody (Methods). Tubulin was used as a loading
656 control. The loading control (anti-tubulin) was run on a different gel/membranes loaded with the
657 same protein sample and treated and analysed in the same manner. The images were cropped
658 showing all relevant bands. (d) Number of body bends per second (BBPS) of N2, WT
659 α Syn::YFP, Δ P1::YFP and $\Delta\Delta$::YFP animals from Day 0 (L4 stage) through to Day 13 of adulthood. Data
660 shown are mean and s.e.m. for three independent experiment; in each experiment, 10 worms were
661 assessed for each time point. n=10 for each experiment and error bars represent SEM of three
662 biological replicates. n.s. = not significant; **P<0.01; *P<0.05, a one-sided test was used. Data for
663 graphs in b-d are available as Source Data.

664

665 **Figure 7. Lipid-induced aggregation kinetics of WT α Syn and its variants.** a-c Far-UV CD
666 spectra of 25 μ M WT α Syn (a), $\Delta\Delta$ (b) or P1P2-GS (c) incubated with increasing ratios of
667 [DMPS]:[protein]. K_D and L values were calculated from the change in MRE at λ_{222nm} fitted to a single
668 step binding model⁶¹ (Extended Data Figure 7b). Aggregation kinetics of 50 μ M α Syn WT (d), $\Delta\Delta$ (e)
669 or P1P2-GS (f) incubated with 0:1, 8:1 or 60:1 [DMPS]:[protein] (20 mM sodium phosphate, pH 6.5;
670 30 °C, no shaking). g-j TEM images of representative samples of WT α Syn (g), $\Delta\Delta$ (h) or P1P2-GS (i) at
671 the endpoint of the incubations (150 h) in the presence of 60:1 [DMPS]:[protein]. Data for graphs in
672 a-f are available as Source Data.

673

674 **Figure 8. NMR experiments detailing the molecular basis of liposome binding of WT α Syn**
675 **$\Delta\Delta$ and P1P2-GS.** ¹H-¹⁵N HSQC NMR spectra of a) WT α Syn, b) $\Delta\Delta$ and c) P1P2-GS in the presence
676 (green) or absence (orange) of a 60:1 ratio of [DMPS]:[protein]. d) Intensity ratios (presence/absence
677 of liposomes) of cross-peaks for WT α Syn (blue), $\Delta\Delta$ (red) and P1P2-GS (orange) are shown by
678 illustrating the median value over a rolling window of five residues determined using OriginPro. The
679 position of P1 and P2 is highlighted with grey bars. Note that residues 36-42 and 45-57 are deleted in
680 $\Delta\Delta$ and these residues (replaced with (SG)₃S (P1) and (GS)₆G (P2)) could not be assigned for P1P2-GS.
681 Data for graph in d are available as Source Data.

682

683 **Methods**

684 **Mutagenesis, expression and purification**

685 α Syn containing single Cys variants, the P1P2-GS control (P1 (7 aa) replaced with (SG)₃S and P2 (13
686 aa) with (GS)₆G) and/or deletions of C1, P1 and/or the P2 regions were engineered into the gene
687 sequence for WT α Syn via Q5 site directed mutagenesis (NEB). ¹⁴N, ¹⁵N and ¹³C/¹⁵N labelled α Syn
688 variants were expressed recombinantly in *Escherichia coli* BL21 (DE3) cells and the protein purified
689 as described previously⁷⁰. In the case of ¹⁵N and/or ¹³C labelled protein, expression was performed in
690 HCDM1 minimal medium with ¹⁵N enriched NH₄Cl and ¹³C enriched glucose. Note that by contrast
691 with Masuda *et al.*⁷¹ there was no evidence of mis-incorporation of Cys for Try at residue 136, as the
692 correct molecular masses of all proteins were confirmed by mass spectrometry (WT: 14 459 ± 0.27
693 Da; Δ P1: 13 784 ± 0.50 Da; Δ P2: 13 182 ± 0.96 Da; $\Delta\Delta$: 12506 ± 0.03 Da; Δ C1: 13 861 ± 0.56 Da; P1P2-
694 GS: 13947.4 ± 0.06 Da) (spectra are available at <https://doi.org/10.5518/707>). Additionally, the NMR
695 spectrum of all proteins was fully assigned with residue 136 being confirmed as Tyr. Proteins were
696 lyophilised and stored at -20°C. Proteins were resolubilised in buffer immediately before
697 experiments were carried out. There was no evidence for covalent dimers forming during storage
698 (samples were analysed before and after storage by ESI-MS). Different buffer conditions were used
699 to analyse the behaviour of the proteins at pH 7.5 (20mM Tris HCl) or pH 4.5 (20 mM sodium
700 acetate), with high (200 mM NaCl) or low (20 mM NaCl) salt concentrations. The isoelectric points of
701 the protein variants are: WT: 4.67; Δ P1: 4.67; Δ P2: 4.60; $\Delta\Delta$: 4.60; Δ C1: 4.72; P1P2-GS: 4.60
702 (calculated using ProtParam tool from ExPASy).

703 ***In silico* methods to determine aggregation propensity**

704 The aggregation propensity was analysed by using the online tools Camsol³⁸, Zyggregator³⁷ and
705 ZipperDB³⁹ at pH 7.0.

706 **Aggregation assays monitored by ThT fluorescence**

707 100 μ L samples of 100 μ M α Syn variants in the required buffers were incubated with 20 μ M ThT in
708 sealed 96-well flat bottom assay plates (Corning, non-binding surface) in a FLUOstar Omega plate
709 reader (BMG Labtech) at 37 °C with continuous orbital agitation at 600 rpm. The fluorescence of ThT
710 was excited at 444 nm and fluorescence emission was monitored at 480 nm. The elongation rate was
711 determined by fitting a gradient to the linear part of the ThT-curve, the lag time was taken as the
712 intercept of the line to the baseline fluorescence signal, using OriginPro software (OriginPro 2018b
713 64Bit). This analysis was performed with a minimum of three replicate experiments. The standard

714 deviations were calculated for repeated measurements (Supplementary Table 1). Fibril yields were
715 determined via centrifugation (30 min 13,000 rpm (Microfuge SN 100/90) and analysis of remaining
716 soluble material compared to the starting material using SDS PAGE. For this, SDS-PAGE gels were
717 imaged on the Alliance Q9 Imager (Uvitec) and band intensities were determined using ImageJ
718 1.52a. Repeat experiments and loading controls indicating an error of ~10% in quantifying band
719 intensity using this approach. Experiments monitoring lipid-induced aggregation were performed as
720 above, except that aggregation was followed under quiescent conditions, 30 °C with a protein
721 concentration of 50 µM. To prepare seeds of WT αSyn, 500 µL of 600 µM αSyn in Tris HCl pH 7.5, 20
722 mM NaCl was stirred with a magnet stirrer at 1200 rpm at 45 °C for 48 h. Fibrils were then sonicated
723 twice for 30 sec with a break of 30 sec at 40 % maximum power using a Cole-Parmer-Ultraprocessor-
724 Sonicator. The resulting seeds (10 % (v/v)) were added to 100 µM monomer and elongation
725 measured in 20 mM Tris HCl, pH 7.5, containing 20 mM NaCl, 20 µM ThT at 37 °C using quiescent
726 conditions.

727 **Negative stain TEM**

728 Samples at ThT incubation endpoints (usually 100 h) were diluted 1 in 10 or 1 in 5 with 18 MΩ H₂O
729 and then applied to carbon coated copper grids in a dropwise fashion. Grids were then dried with
730 filter paper, washed three times with 18 MΩ H₂O in a dropwise fashion, drying with filter paper after
731 each wash, before fibril samples were negatively stained by the addition of 1% (w/v) uranyl acetate,
732 added and blotted twice as before. Images were recorded on a Joel JEM-1400 or FEI Tecnai T12
733 electron microscope.

734 **Preparation of disulfide locked dimeric αSyn species**

735 To allow the formation of disulfide linkages between monomeric αSyn Cys variants, 400 µM αSyn
736 was incubated in 100 mM, Tris HCl, pH 8.4 for 2 h at room temperature. Protein samples were then
737 added to a HiLoad™ 26/60 Superdex 75 preparative grade gel filtration column (GE Healthcare) in
738 50 mM ammonium bicarbonate, pH 8.0, which allowed monomer and dimers to be resolved.
739 Disulfide locked dimeric αSyn was then lyophilised and stored at -20 °C. The presence of disulfide
740 linkages was validated using reducing and non-reducing SDS-PAGE with SEC-MALS used to validate
741 the purification of dimeric constructs. For the latter, 50 µL of a 30 µM sample of αSyn was injected
742 onto a TOSOH G200SWXL column equilibrated with 20 mM Tris HCl, containing 200 mM NaCl, pH
743 7.5. The protein peak was eluted into a Wyatt miniDawnTrosos system with three angle detection and
744 the data analysed using Astra 6.0.3® software supplied with the instrument.

745

746 **NMR Backbone assignments of WT α Syn, α Syn P1P2-GS and α Syn $\Delta\Delta$**

747 WT and $\Delta\Delta$ α Syn variants were $^{13}\text{C}/^{15}\text{N}$ uniformly labelled for NMR backbone assignments purposes.
748 200 μM of protein in 20 mM sodium acetate, 20mM NaCl, 10% (v/v) D_2O , 0.02% (w/v) sodium azide,
749 pH 4.5 at 15 $^\circ\text{C}$ was used to acquire triple correlation experiments: HNCO, HNcaCO, HNCACB,
750 HNcoCACB, HNN-TOCSY, hNcaNNH and hNcaNNH. All experiments were acquired using non-uniform
751 sampling, where just 45% of sparse data was recorded on a Bruker AVANCE III 750 MHz
752 spectrometer equipped with a triple resonance TCI-cryoprobe.

753 NMR data processing and spectra reconstruction were performed using NMRpipe⁷² and data analysis
754 with ccpNMR-Analysis software⁷³. HN, C_α and C_β chemical shifts were deposited at Biological
755 Magnetic Resonance Bank (BMRB) with access numbers 27900, 27901 and 28045 for WT α Syn, $\Delta\Delta$
756 and P1P2-GS, respectively.

757 **Paramagnetic Relaxation Enhancement NMR experiments**

758 α Syn Cys variants were incubated with 5 mM DTT in 20 mM Tris HCl, 200 mM NaCl, pH 7.5 for 30
759 min. DTT was then removed by a Zeba spin column (PD10 column, GE Healthcare) and the sample
760 labelled immediately by incubation with a 40-fold molar excess MTSL for 16 h at 4 $^\circ\text{C}$ in 20 mM Tris
761 HCl, 200 mM NaCl, pH 7.5. Excess spin label was removed by Zeba spin column (PD10 column) and
762 protein eluted in the required buffer. Spin-labelled α Syn constructs were used directly or stored at -
763 80 $^\circ\text{C}$. In all cases 100 % labelling at a single site was confirmed using ESI-MS. For intramolecular PRE
764 experiments, ^1H - ^{15}N HSQC spectra were obtained using 100 μM ^{15}N spin labelled α Syn in 20 mM
765 acetate buffer pH 4.5 containing 20 mM or 200 mM NaCl, 10% (v/v) D_2O , 0.02% (w/v) sodium azide
766 on an AVANCE III Bruker spectrometer (600 MHz) equipped with a triple channel QCI-P cryoprobe.
767 All NMR experiments were carried out at 15 $^\circ\text{C}$. Diamagnetic spectra were obtained following the
768 addition of 2 mM ascorbic acid. Note that small changes in chemical shift occur upon adding this acid
769 to the protein spectra and reduction was not complete, leading to small residual intensity of some
770 resonances in the spectra especially when MTSL was added to A90C (see legend to [Extended Data](#)
771 [Figure 4](#)). Note that this does not affect the conclusions drawn since it underestimates, rather than
772 overestimates the magnitude of the PRE measured. Spectra were processed in Topspin (Bruker)
773 using CCPN⁷⁴. Peak heights were used to calculate intensity ratios (paramagnetic/ diamagnetic).
774 Control experiments in which 50 μM ^{15}N α Syn and ^{14}N α Syn-MTSL were mixed showed no PREs,
775 ruling out intermolecular interactions at this protein concentration under the conditions used. PRE
776 effects arising from non-specific binding of the hydrophobic probe MTSL to α Syn was ruled out by
777 performing experiments in which 100 μM free MTSL was added to 100 μM ^{15}N α Syn WT (lacking Cys)
778 in which no PREs were observed. Replicate measurements of the PRE intensity ratios (I/I_0) using

779 different preparations of WT α Syn in high and low salt conditions enabled per-residue errors to be
780 determined. On average these were +/- 0.05. These data are available in
781 (<https://doi.org/10.5518/707>). Intermolecular PRE experiments were carried out by mixing 250 μ M
782 15 N WT or $\Delta\Delta$ α Syn with 250 μ M 14 N-MTSL labelled protein. T_2 transverse relaxation experiment was
783 performed based in HSQC pulse sequence⁷⁵ with 10 T_2 delays (from 16.96 to 610.56 ms), under
784 paramagnetic and diamagnetic conditions. Data processing was performed using NMRpipe⁷². Cross
785 peaks intensities at each T_2 -delay were analysed using PINT and fitted to a single exponential decay
786 using PINT. The effective H_N - Γ_2 rate was calculated as the difference between the R_2 rate in the
787 paramagnetic versus the diamagnetic samples (Equation 1):

$$\Gamma = R_{2,para} - R_{2,dia} \quad \text{Eq. 1}$$

788 **Maintenance and generation of transgenic *C. elegans* strains and *in vivo* aggregation** 789 **measurements**

790 The WT α Syn gene used was fused C-terminally to YFP in vector pPD30.38³⁴. This vector was
791 modified to delete amino acids 36-42 (Δ P1) or residues 36-42 and 45-57 ($\Delta\Delta$) by PCR mutagenesis.
792 Transgenic *C. elegans* expressing each construct were then generated by microinjection of
793 Δ P1 α Syn::YFP or $\Delta\Delta\alpha$ Syn::YFP constructs into the germline of N2 nematodes, resulting in strains
794 PVH214 *pccEx021[unc-54p::a-synuclein Δ P1::YFP]* and PVH198 *pccEx001[unc-54p::a-synuclein*
795 *Δ P1 Δ P2::YFP]* (Nemamatrix). Nematodes expressing WT α syn::YFP were created using gene
796 bombardment and kindly provided by Ellen Nollen³⁴.

797 For imaging, *C. elegans* was cultured on NGM plates seeded with *E. coli* OP50-1 at 20 °C as described
798 previously⁷⁶. *C. elegans* was imaged using a Zeiss LSM880 confocal fluorescent microscope through a
799 10x 1.0 or a 20x 1.0 numerical aperture objective with a 514 nm line for excitation of YFP. Before
800 imaging, age-synchronised animals at different ages (Day 0 (L4 stage) to Day 13) were anaesthetised
801 using 5 mM Levamisole solution in M9 buffer and mounted on 2% (w/v) agar pads. The number of
802 α Syn::YFP foci were then counted and the mobility of all foci in at least 10 animals per time point
803 and in three independent cultures of *C. elegans* (biological replicates) was determined using FRAP, as
804 described previously³⁴. Note that the higher expression levels of the Δ P1 and $\Delta\Delta$ constructs does not
805 affect the FRAP analysis, as FRAP measures relative fluorescence intensities of similar size photo-
806 bleached and unbleached regions within the same animal.

807 To determine motility of the worms, a total of 30 age-synchronised animals were used for each assay
808 and each experiment was repeated at least three times. Animals were moved into M9 buffer at
809 indicated time points (Day 0 through to Day 13 of adulthood) and thrashing rates were measured by

810 counting body bends for 15 s using the wrMTrck plugin for ImageJ (available at
811 <http://www.phage.dk/plugins/wrmtrck.html>)⁷⁷. Error bars represent SEM of three biological
812 replicates.

813 **Immunoblotting**

814 Nematodes were collected from plates, washed in M9 buffer, and resuspended in lysis buffer (20
815 mM Tris HCl, pH 7.5; 10 mM β -mercaptoethanol; 0.5% (v/v) Triton X-100; supplemented with
816 complete protease inhibitor (Roche) before shock freezing in liquid nitrogen. Three freeze-thaw
817 cycles were performed before the worm pellet was ground with a motorized pestle, and lysed on ice,
818 in the presence of 0.025 U/mL benzonase (Sigma). The lysate was centrifuged at 1000 rpm for 1 min
819 in a table top centrifuge to pellet the carcasses. Protein concentration was determined using
820 Bradford assay (Bio-Rad). Samples were then mixed 1:1 with SDS loading buffer (2% (w/v) SDS, 10 %
821 (v/v) glycerol, 0.1 % (w/v) bromophenol blue, 100 mM DTT), boiled for 10 min and 25 μ g final
822 protein was loaded onto a 4-20% gradient Tris HCl gel (Bio-Rad). Protein bands were blotted onto a
823 PVDF membrane and α Syn and tubulin (control) were visualised using a mouse anti- α Syn antibody
824 (syn211 (1:5000) (NeoMarkers)) or mouse anti-tubulin antibody (1:5000) (Sigma), followed by an
825 anti-mouse horse-radish peroxidase-coupled secondary antibody (1:5000). Bands were visualised
826 using the SuperSignal West Pico Plus Chemiluminescence Substrate (Thermo).

827 **Liposome preparation**

828 1,2-dimyristoyl-sn-glycero-3-phospho-L-serine (DMPS) (sodium salt, Avanti Polar Lipids) was
829 dissolved in 20 mM sodium phosphate buffer, pH 6.5 and stirred at 45 °C for 2 h. The solution was
830 then frozen and thawed 5-times using dry ice and a water bath at 45 °C, respectively. Preparation of
831 liposomes was then carried out by sonication in a bath sonicator (U50 ultrasonic bath, Ultrawave) for
832 1 h. The sizes of liposomes were measured using dynamic light scattering (DLS). For DLS 250 μ L of
833 100 μ M samples were injected into a Wyatt miniDawnTreas system (equipped with an additional
834 DLS detector) and the data analysed using Astra 6.0.3[®] software supplied with the instrument.
835 Filtered (0.22 μ m) and de-gassed buffer, kept cool on ice to minimise bubble formation inside the
836 instrument, was used to obtain 5 min baselines before and after sample injection. A 3 min sample
837 window was used for the analysis by the software. Using this analysis the liposomes were found to
838 have a diameter \approx 160 nm.

839 **CD spectroscopy and lipid binding experiments**

840 CD samples were prepared by incubating 25 μ M WT α Syn, $\Delta\Delta$ or P1P2-GS with different

841 concentrations of DMPS liposomes in 20 mM sodium phosphate buffer, pH 6.5. Far-UV CD spectra
 842 were acquired in in 1 mm path length quartz cuvettes (Hellma) using a Chirascan™ plus CD
 843 Spectrometer (Applied Photophysics). CD spectra were acquired using a 2 nm bandwidth, 1 s time
 844 step, data collected at 1 nm increments at 30 °C. An average of 3 scans (190-260 nm) were acquired
 845 per sample. The data were fitted to determine the secondary structure content using Dichroweb⁷⁸.

846 K_D and stoichiometry values were calculated from CD data using the protocol described in⁶¹ using the
 847 fitting function shown in Equation 2:

$$x_B = \frac{\left(\left([\alpha\text{Syn}] + \frac{[\text{DMPS}]}{L} + K_D \right) - \sqrt{\left(\left([\alpha\text{Syn}] + \frac{[\text{DMPS}]}{L} + K_D \right)^2 - \frac{4[\text{DMPS}][\alpha\text{Syn}]}{L} \right)} \right)}{2[\alpha\text{Syn}]} \quad \text{Eq. 2}$$

848 where X_B is the fraction of αSyn bound to the membrane, L represents the number of DMPS
 849 molecules interacting with one molecule of $\alpha\text{-Syn}$ and can be described as:

850

$$851 \quad [\text{DMPS}] = L([\text{DMPS}_L] + [B(\text{DMPS}_L)]) \quad \text{Eq. 3}$$

852 where B is the amount of αSyn bound to liposomes and L is the number of DMPS molecules
 853 interacting with one molecule of $\alpha\text{-Syn}$.

854 **NMR experiments to monitor liposome binding**

855 ¹H-¹⁵N HSQC NMR spectra were obtained using 25 μM ¹⁵N WT αSyn , P1P2-GS or $\Delta\Delta$ αSyn in the
 856 absence or presence of 60:1 [DMPS]:[αSyn] ratios. Experiments were carried out in 20 mM sodium
 857 phosphate, pH 6.5 (as in⁶¹) containing 10% (v/v) D₂O, 0.02% (w/v) sodium azide on an AVANCE III
 858 Bruker spectrometer (600 MHz) equipped with a cryogenic probe. All NMR experiments were carried
 859 out at 20 °C. Published assignments were used to analyse the data (BMRB 16543)⁵⁸. Spectra were
 860 processed in Topspin (Bruker) and analysed in CCPN. Peak heights were used to calculate intensity
 861 ratios of αSyn in the presence versus in the absence of liposomes.

862 Further information on experimental design is available in the Nature Research Reporting Summary
 863 linked to this article

864 **Data availability**

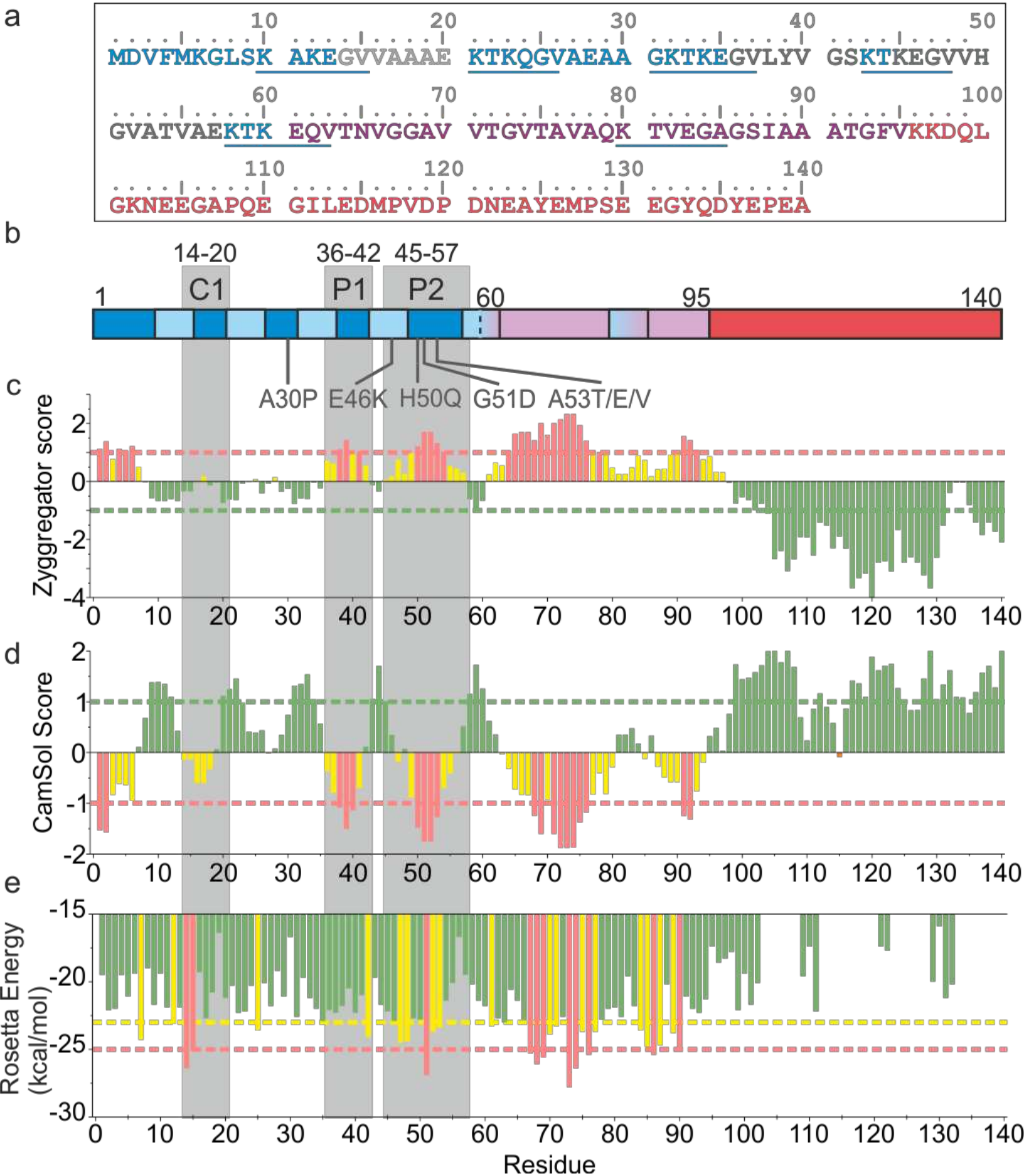
865 Chemical shift assignments can be accessed using BMRB numbers 27900 (WT- αSyn), 27901 ($\Delta\Delta$
 866 αSyn) and 28045 (P1P2-GS αSyn). Source data for Figure 1c-e, Figure 2a-d, Figure 3a-c, Figure 4a-g,

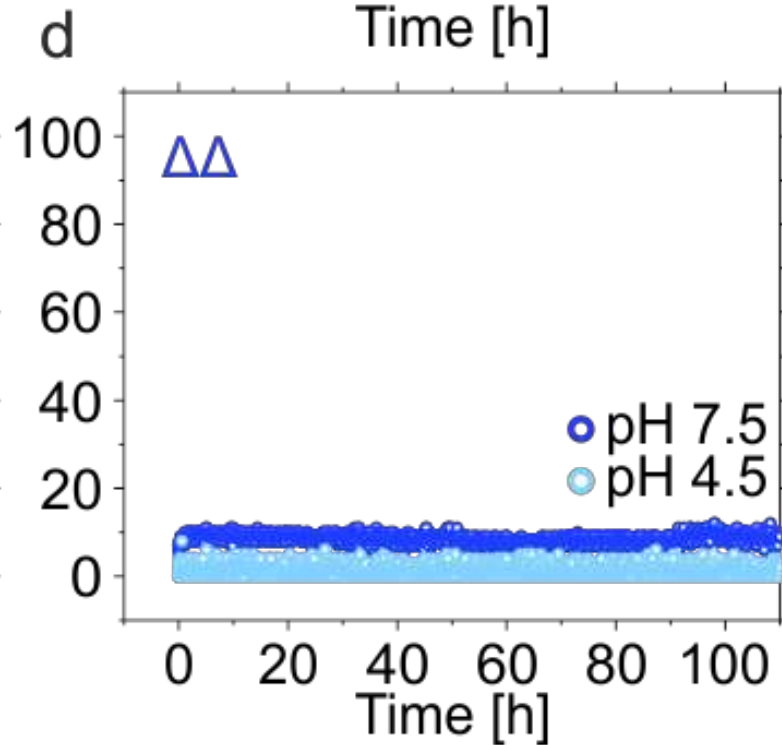
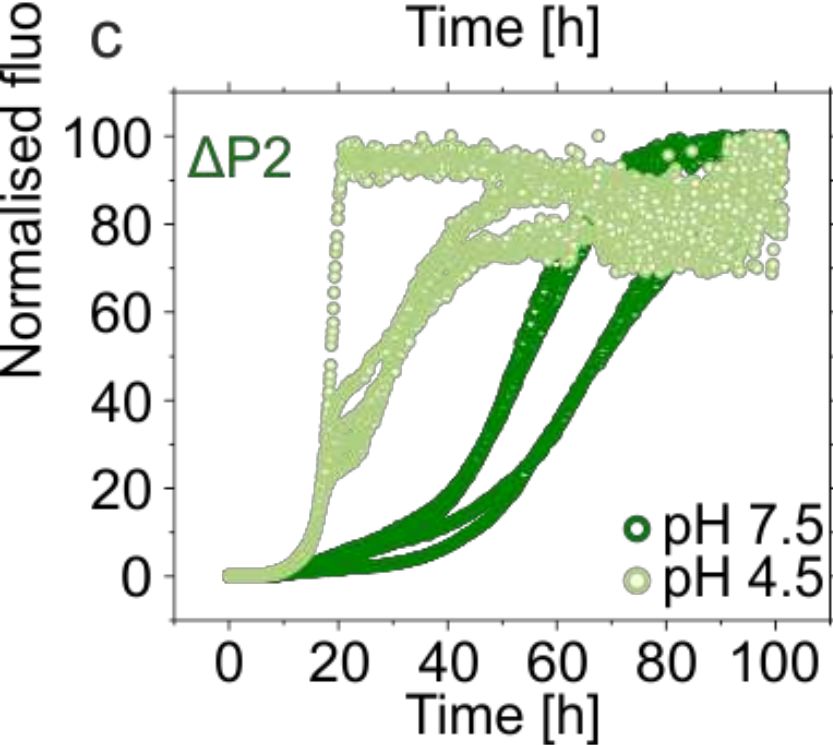
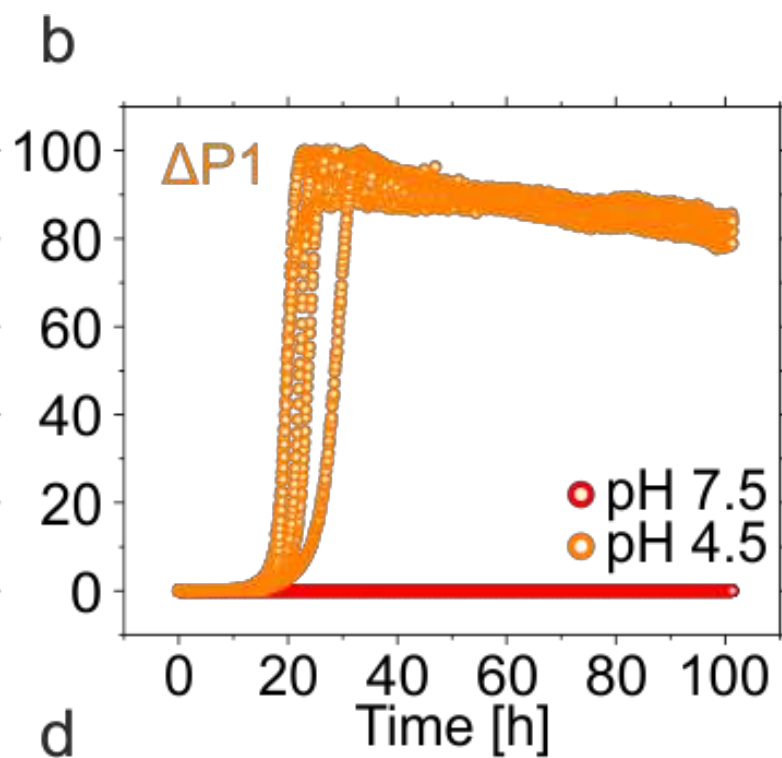
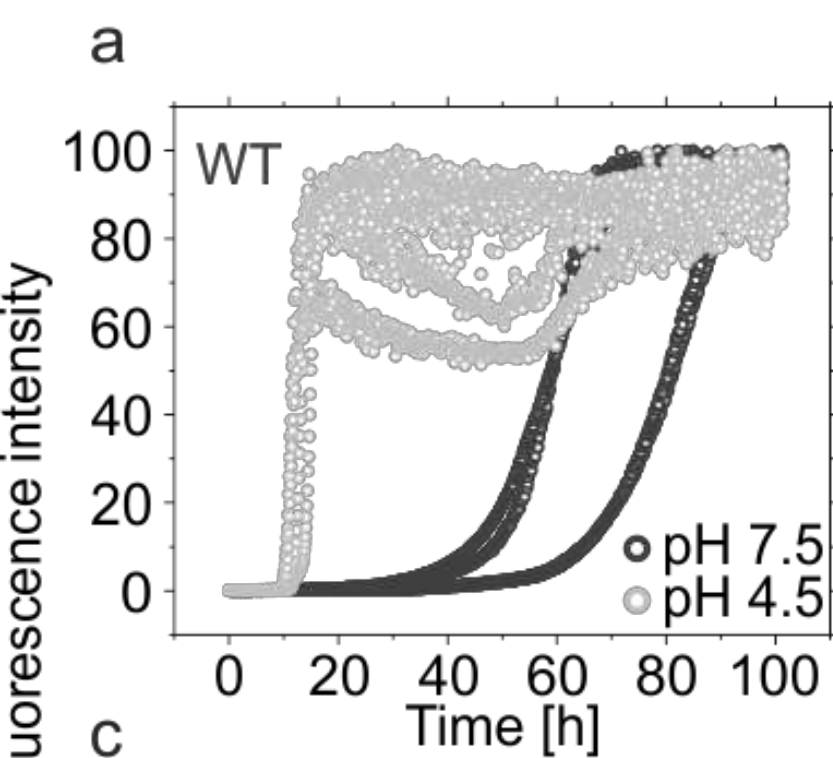
867 Figure 5a-g, Figure 6b,d, Figure 7a-f and Figure 8d and Extended Figure 1a-h, Extended Figure 2a,
868 Extended Figure 3b-g, Extended Figure 5a,b, Extended Figure 6b,c and Extended Figure 7a-d are
869 available with the paper online. Other datasets generated during and/or analysed during the current
870 study are available in the University of Leeds data repository (<https://doi.org/10.5518/707>).

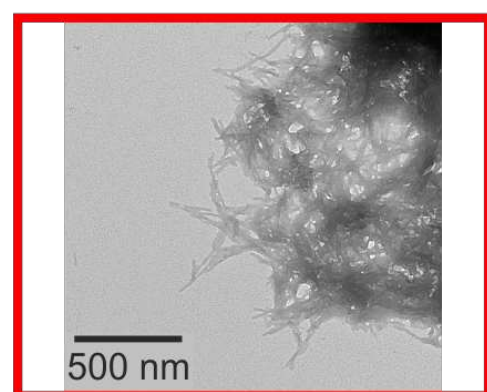
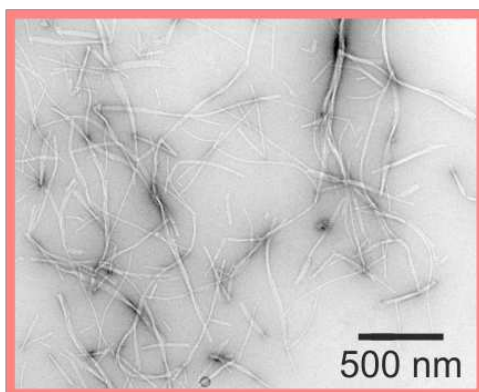
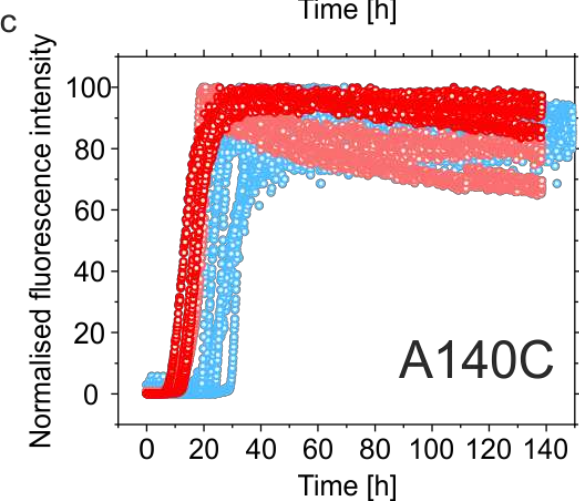
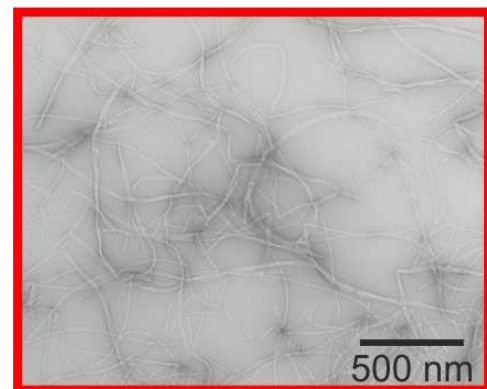
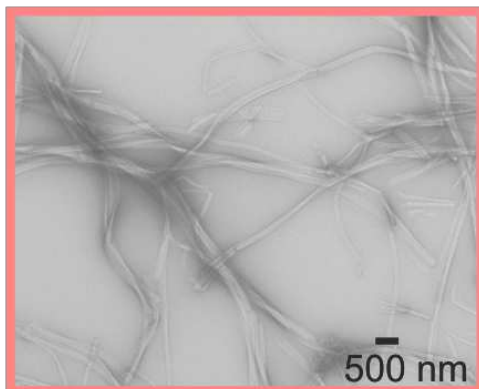
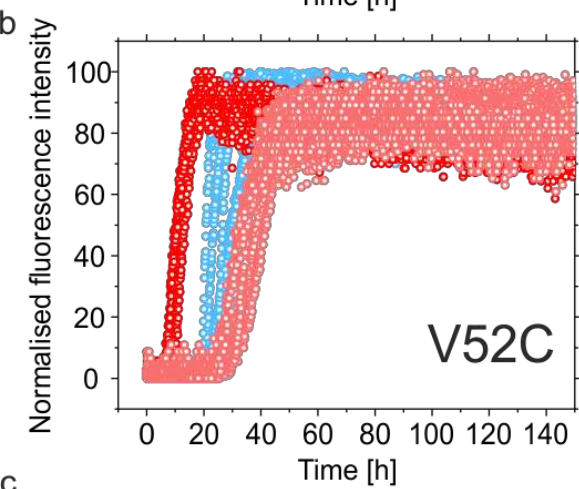
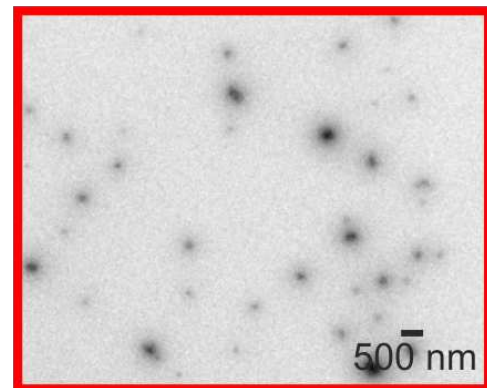
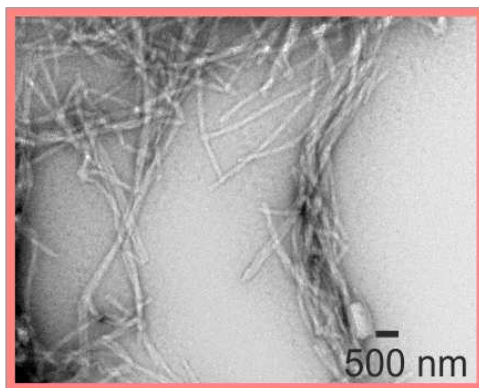
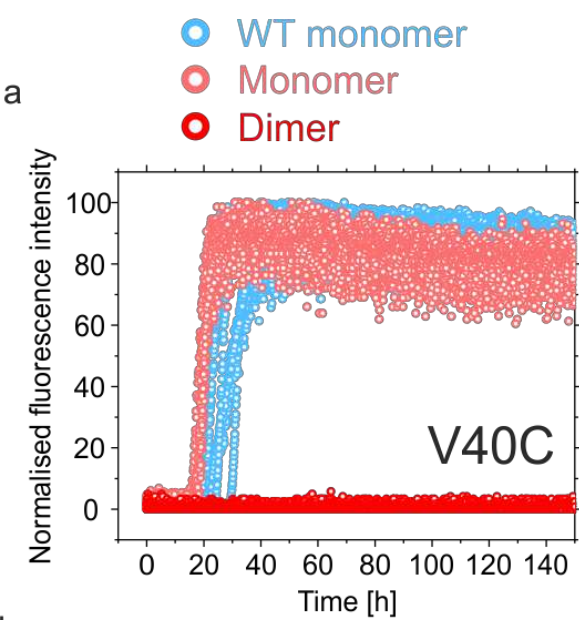
871

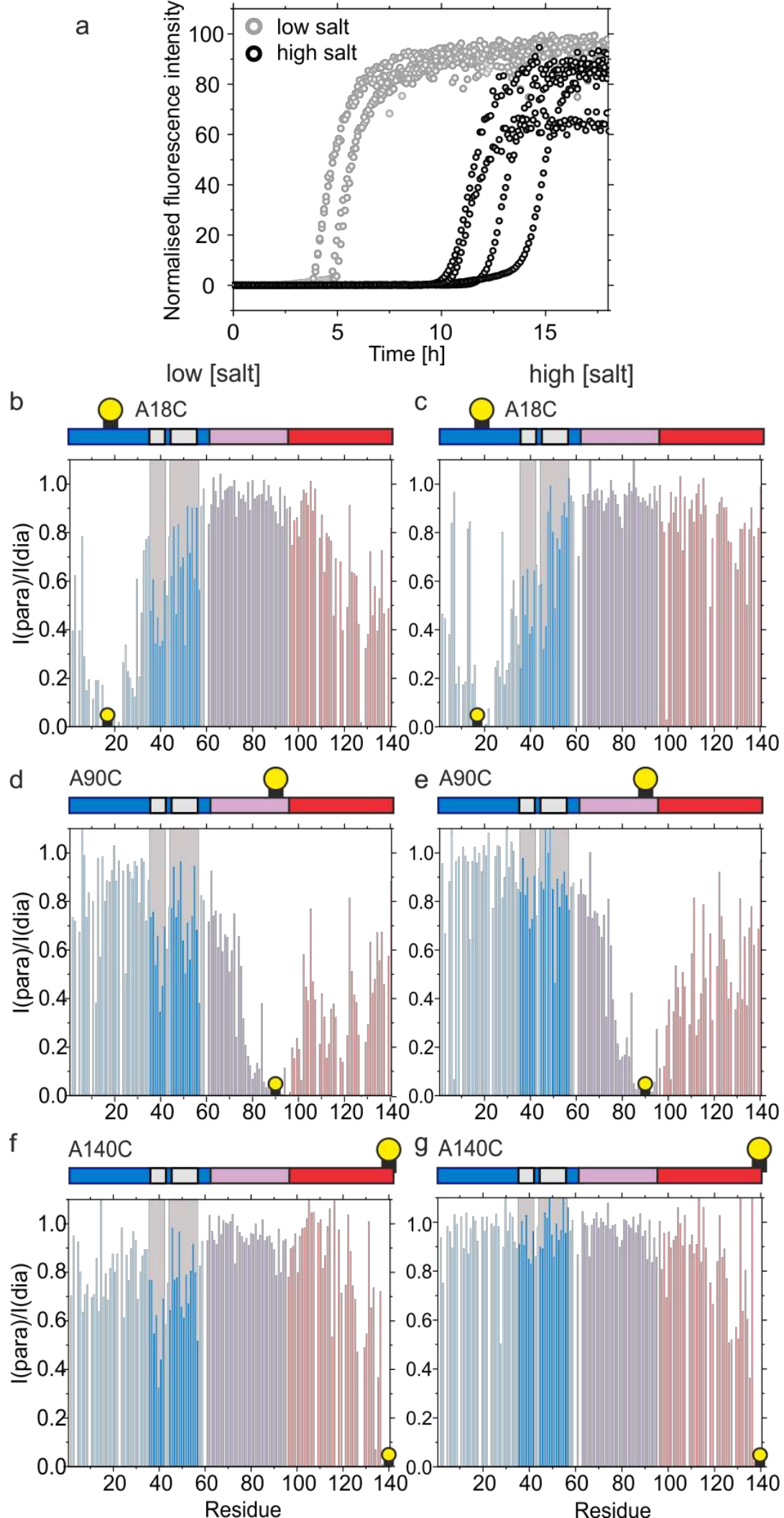
872 **Methods only References**

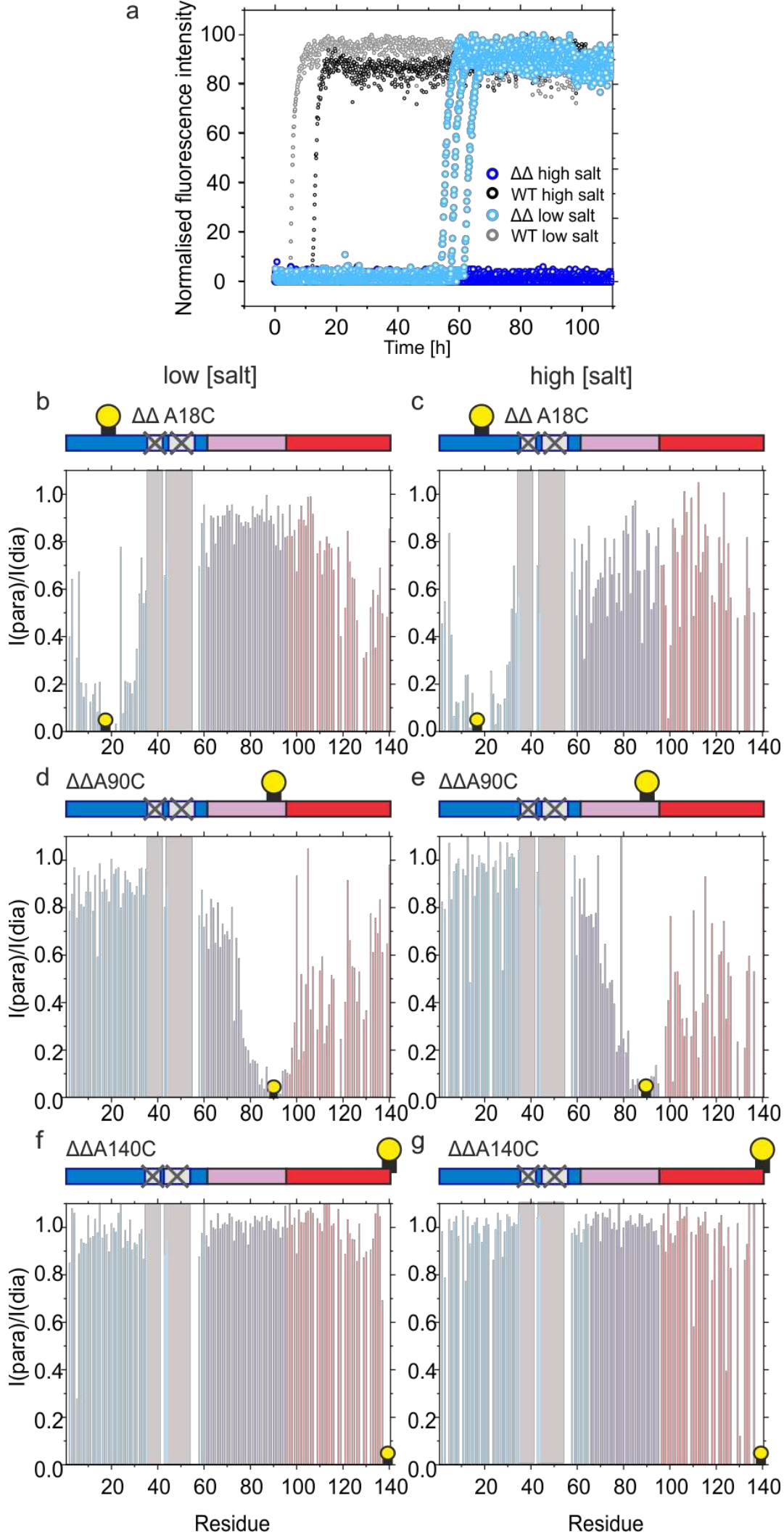
- 873 70. Martin, E.M., Jackson, M.P., Gamberdinger, M., Gense, K., Karamonos, T.K. *et al.*
874 Conformational flexibility within the nascent polypeptide-associated complex enables its
875 interactions with structurally diverse client proteins. *The Journal of biological chemistry* **293**,
876 8554-8568 (2018).
- 877 71. Masuda, M., Dohmae, N., Nonaka, T., Oikawa, T., Hisanaga, S.-i. *et al.* Cysteine
878 misincorporation in bacterially expressed human α -synuclein. *FEBS Lett.* **580**, 1775-1779
879 (2006).
- 880 72. Delaglio, F., Grzesiek, S., Vuister, G.W., Zhu, G., Pfeifer, J. *et al.* NMRPipe: A multidimensional
881 spectral processing system based on UNIX pipes. *J. Biomol. NMR* **6**, 277-293 (1995).
- 882 73. Skinner, S.P., Fogh, R.H., Boucher, W., Ragan, T.J., Mureddu, L.G. *et al.* CcpNmr
883 analysisassign: A flexible platform for integrated NMR analysis. *J. Biomol. NMR* **66**, 111-124
884 (2016).
- 885 74. Fogh, R., Ionides, J., Ulrich, E., Boucher, W., Vranken, W. *et al.* The ccpn project: An interim
886 report on a data model for the NMR community. *Nat. Struct. Mol. Biol.* **9**, 416 (2002).
- 887 75. Tang, C., Schwieters, C.D. & Clore, G.M. Open-to-closed transition in apo maltose-binding
888 protein observed by paramagnetic NMR. *Nature* **449**, 1078 (2007).
- 889 76. Brenner, S. The genetics of *Caenorhabditis elegans*. *Genetics* **77**, 71-94 (1974).
- 890 77. Nussbaum-Krammer, C.I., Neto, M.F., Briemann, R.M., Pedersen, J.S. & Morimoto, R.I.
891 Investigating the spreading and toxicity of prion-like proteins using the metazoan model
892 organism *C. elegans*. *JoVE (Journal of Visualized Experiments)*, e52321 (2015).
- 893 78. Whitmore, L. & Wallace, B. Dichroweb, an online server for protein secondary structure
894 analyses from circular dichroism spectroscopic data. *Nucleic Acids Res.* **32**, W668-W673
895 (2004).

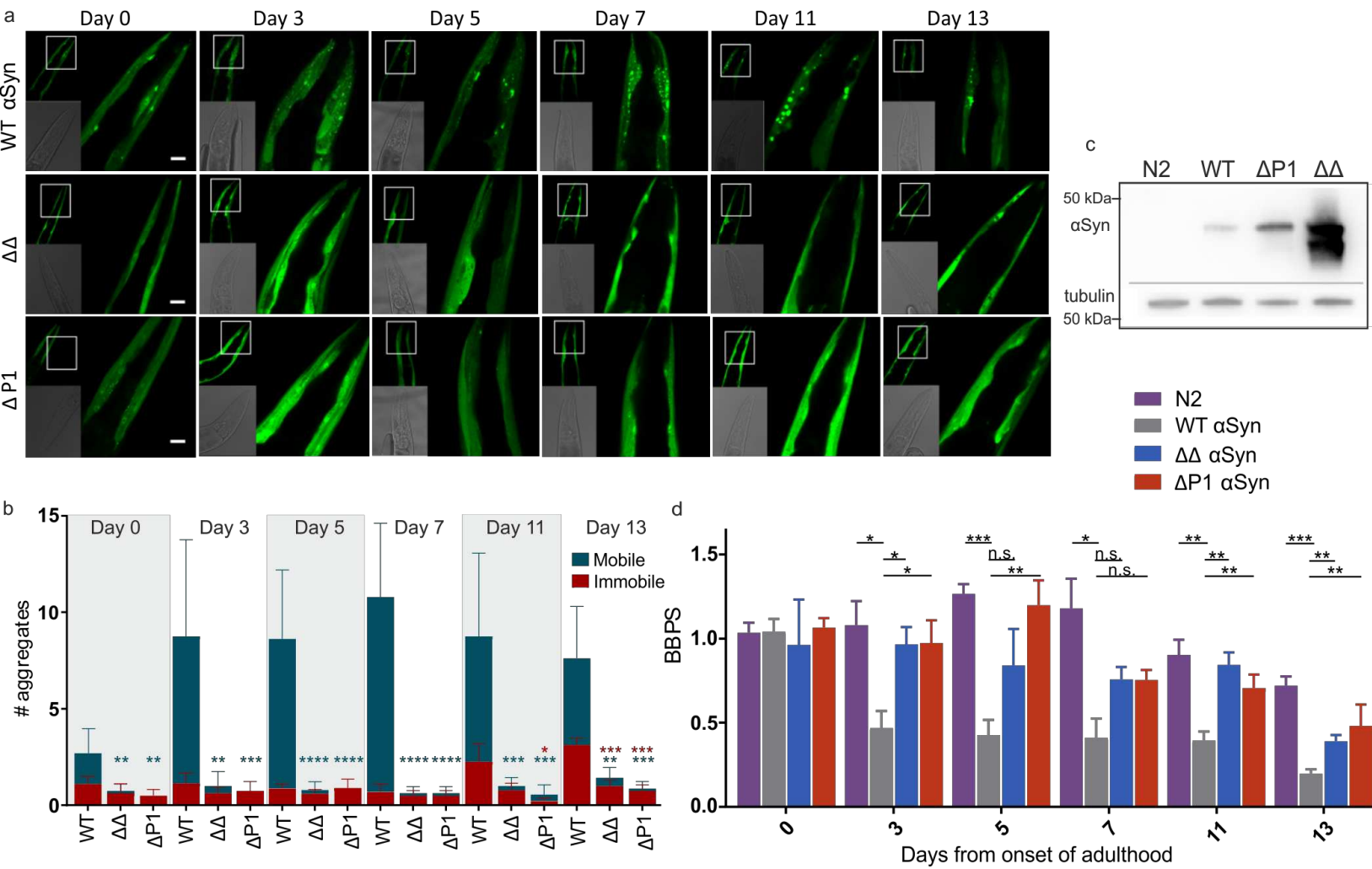


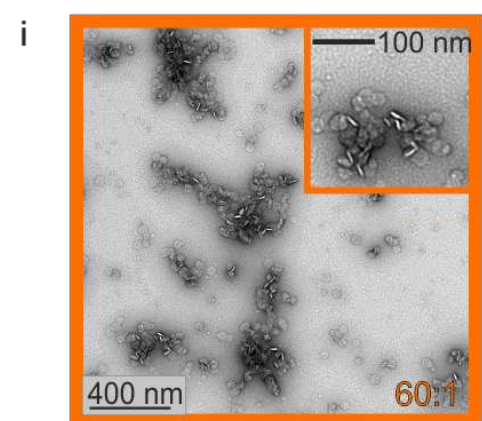
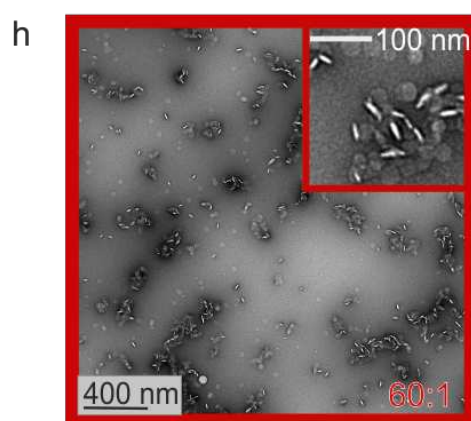
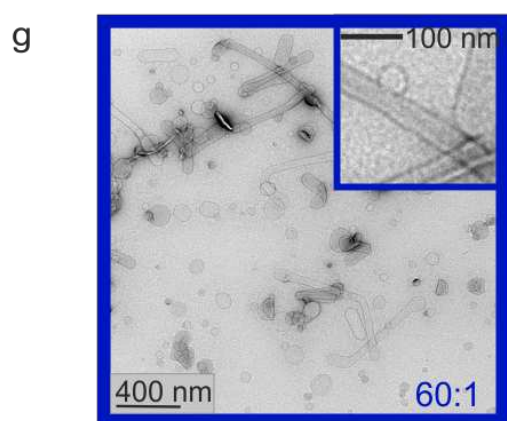
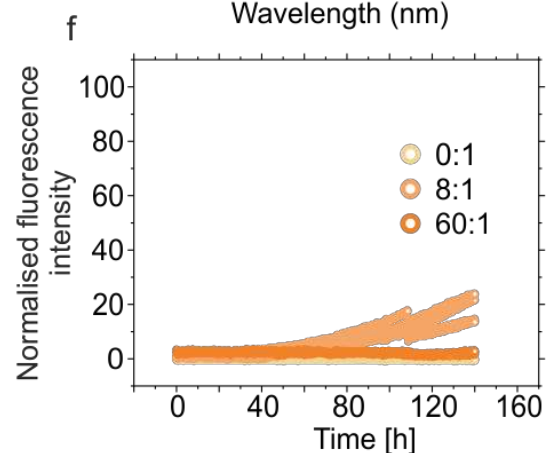
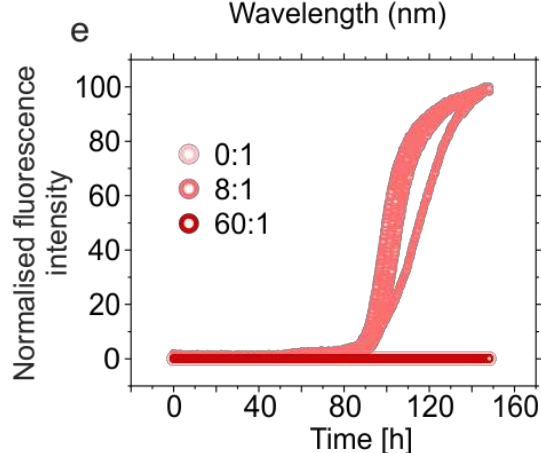
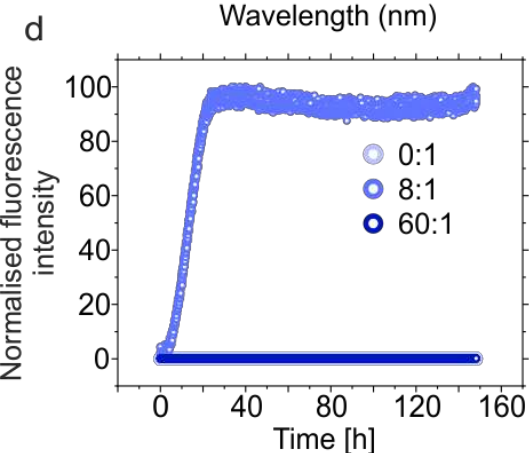
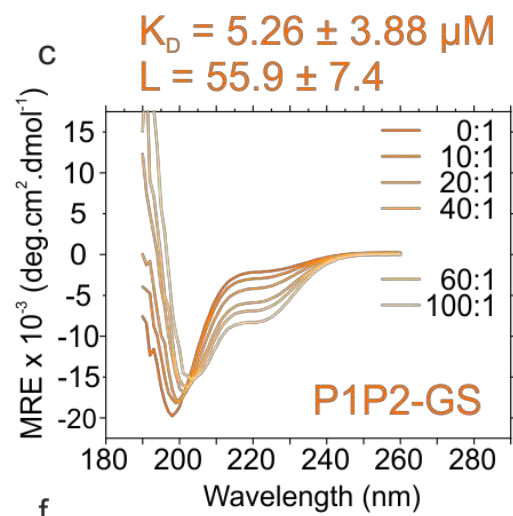
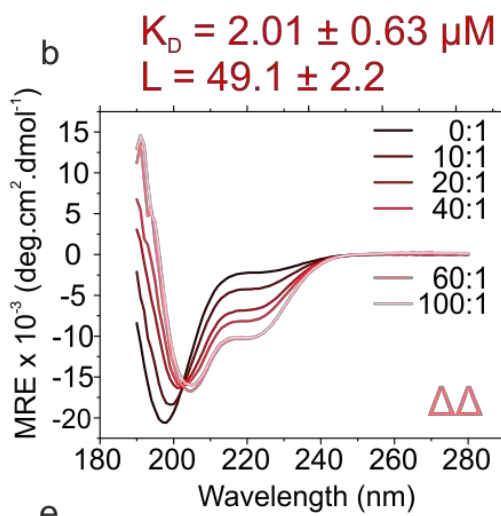
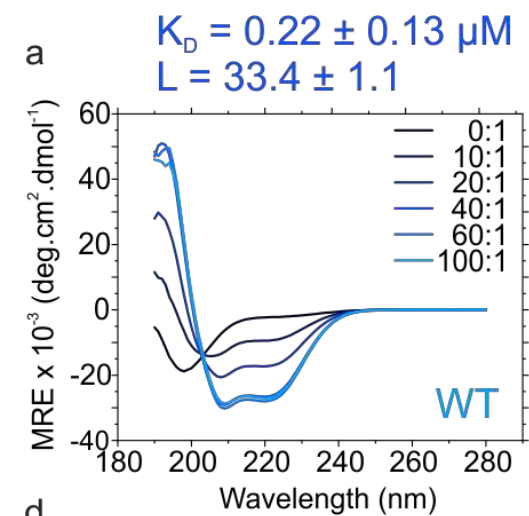


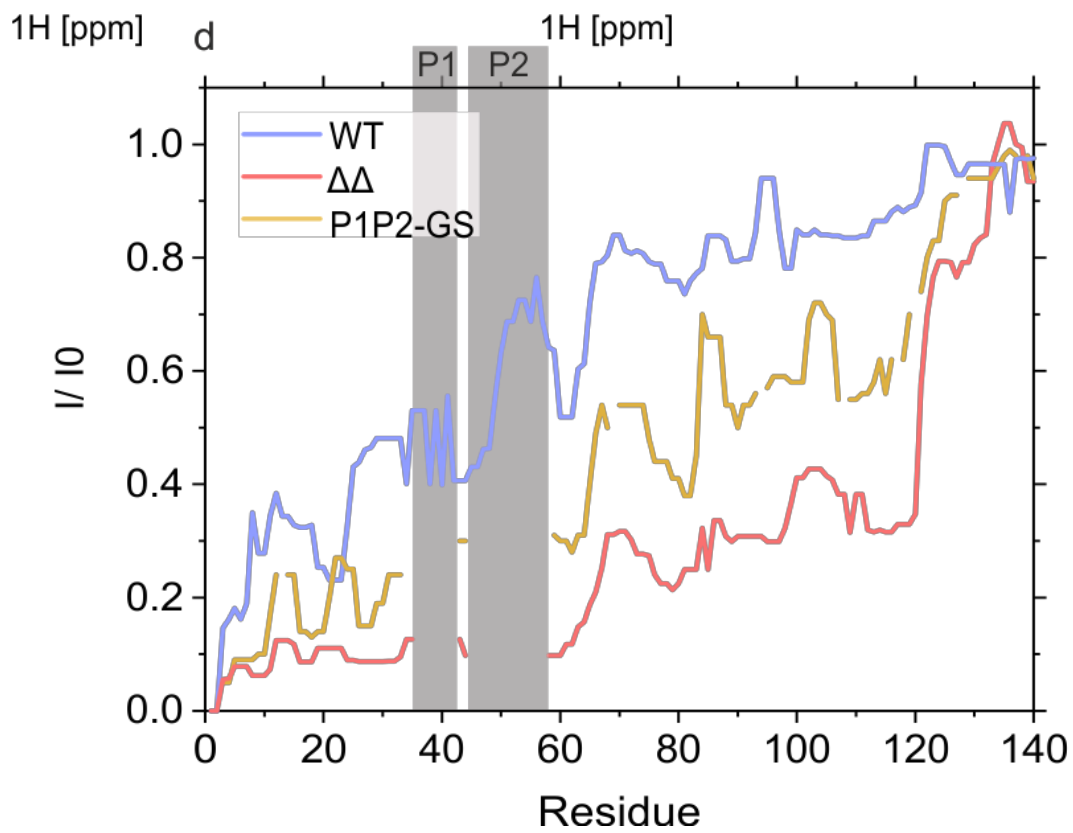
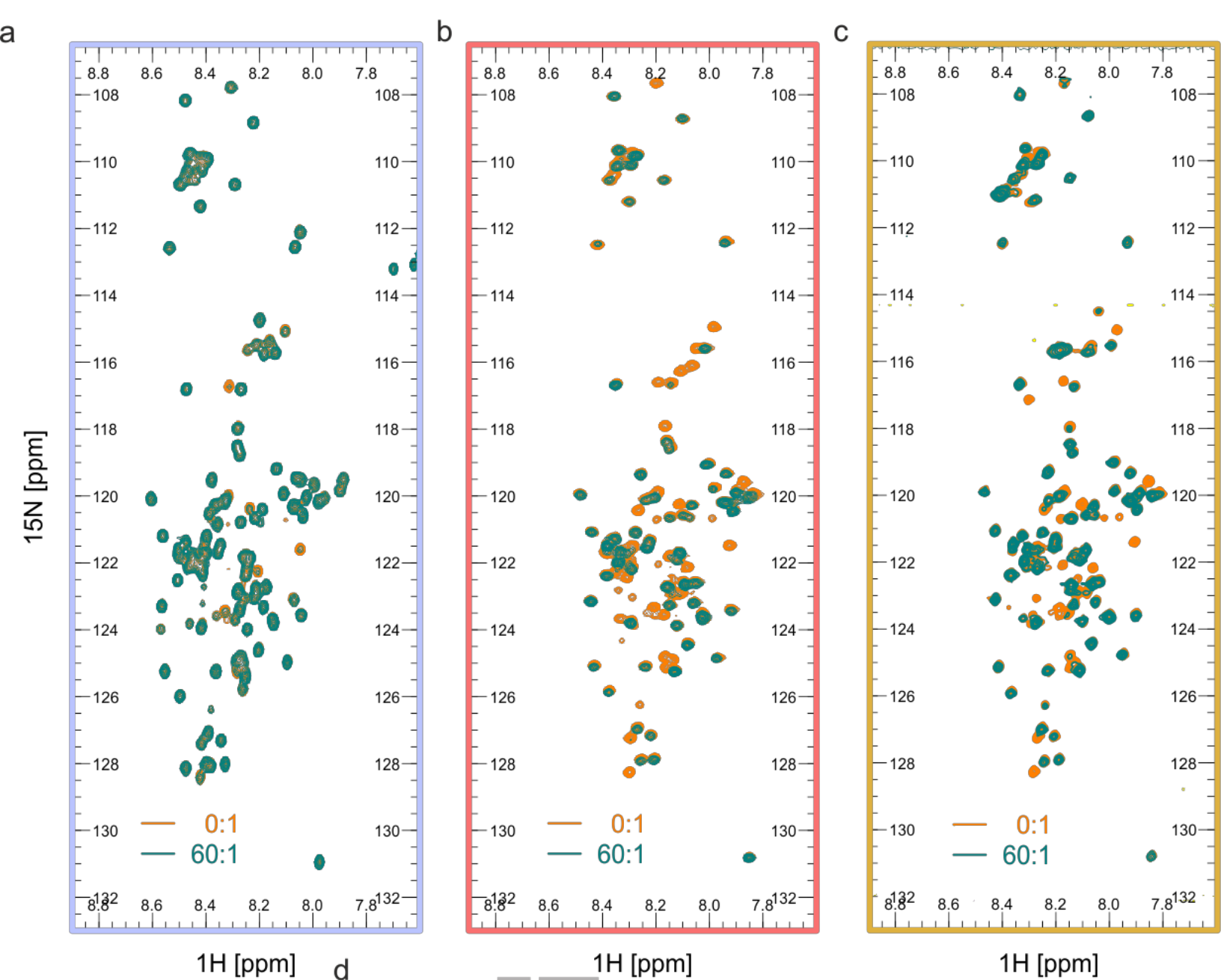


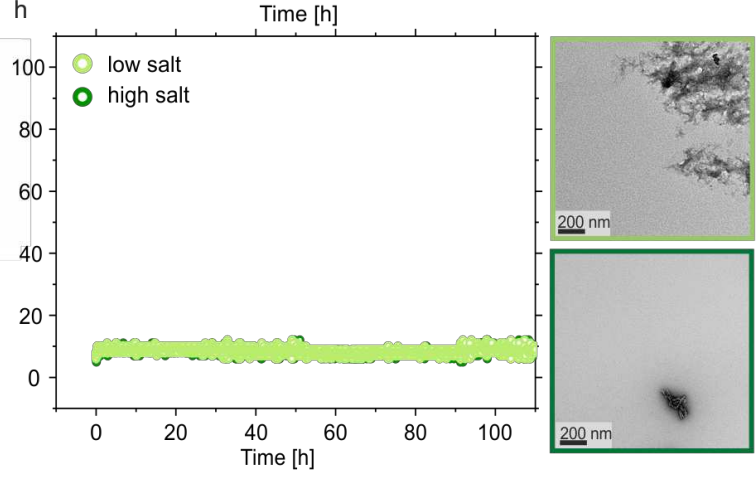
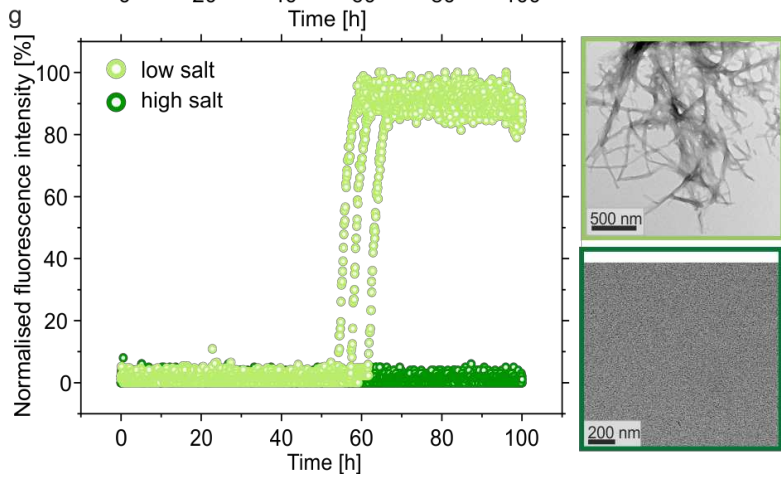
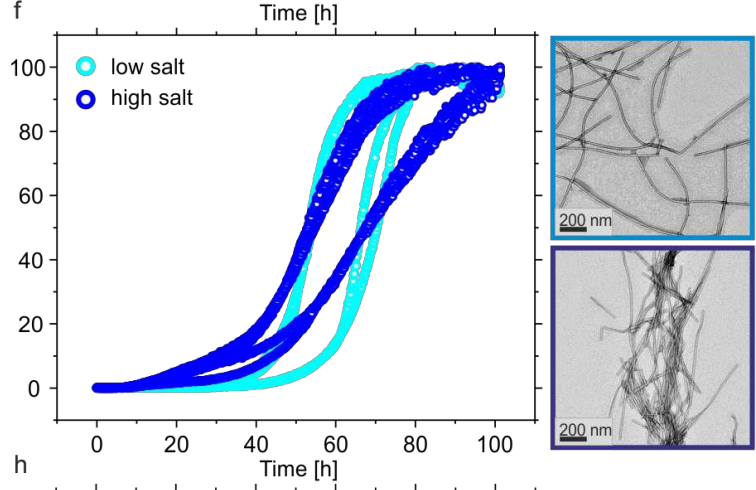
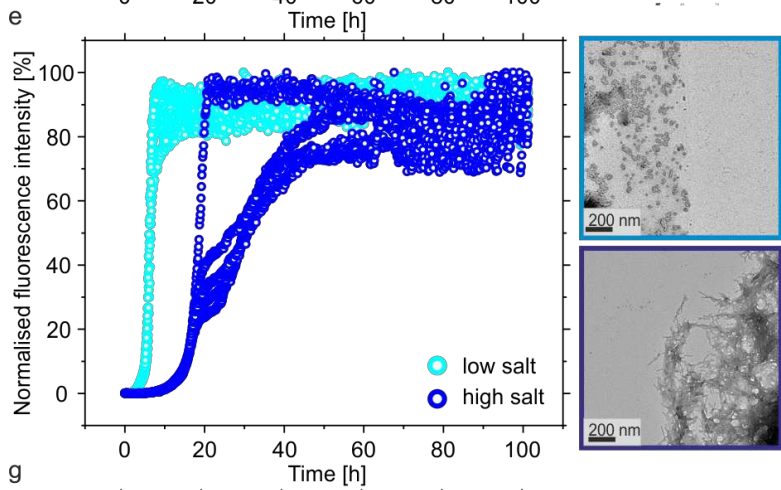
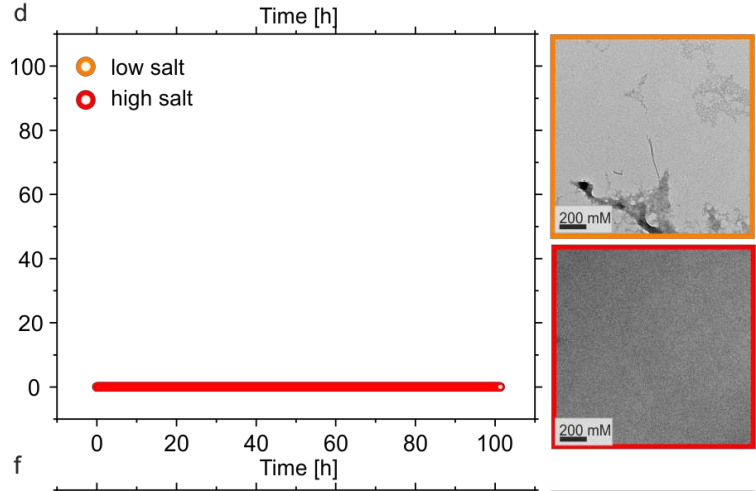
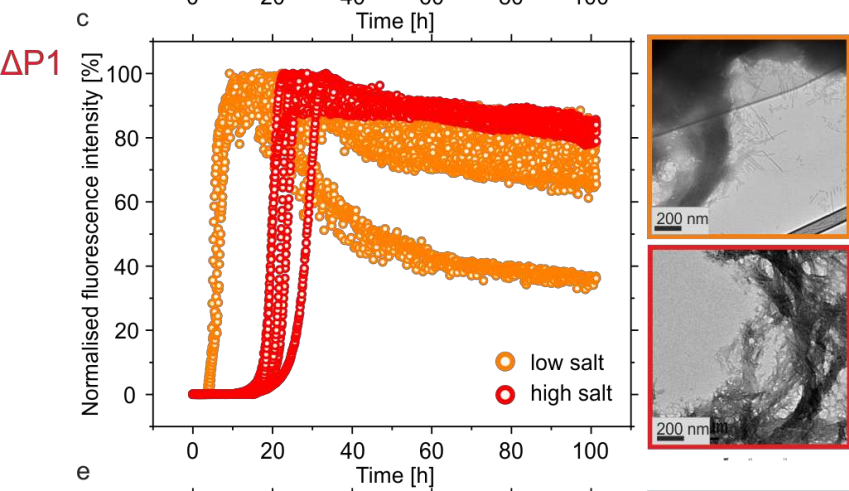
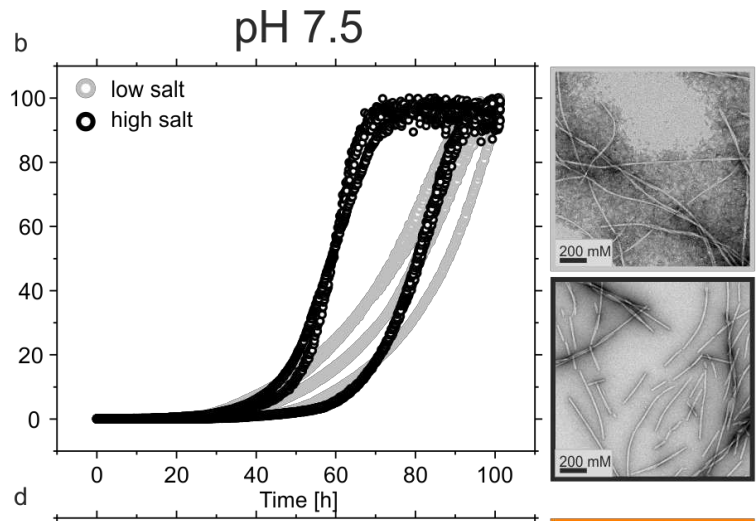
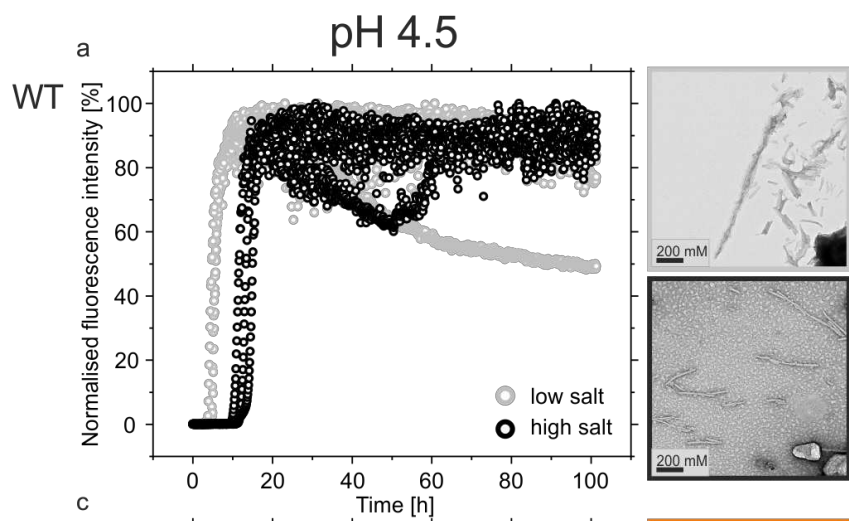




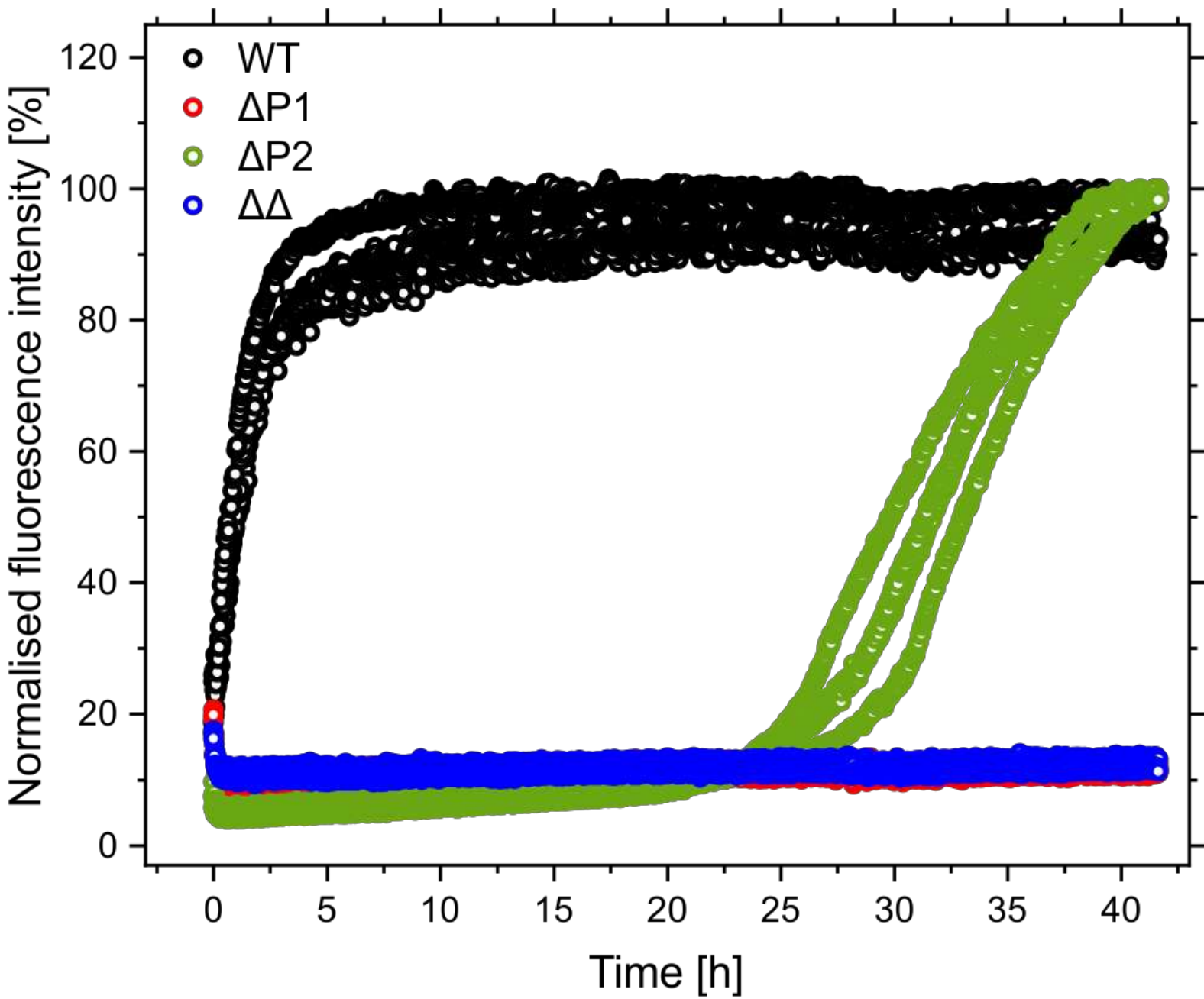








a



b

